1 **Modeling diurnal variation of surface PM$_{2.5}$ concentration over East**

2 **China with WRF-Chem: Impacts from boundary layer mixing and**

3 **anthropogenic emission**

4 [1]Qiuyan Du, [1]Chun Zhao*, [1]Mingshuai Zhang, [1,2]Xue Dong, [1]Yu Chen, [3]Zhen Liu, [4]Zhiyuan

5 Hu, [5]Qiang Zhang, [6]Yubin Li, [1]Renmin Yuan, [7]Shiguang Miao

7 [1]School of Earth and Space Sciences, University of Science and Technology of China, Hefei,

8 China, 230026

9 [2]PowerChina Huadong Engineering Corporation Limited, Hangzhou, China

10 [3]School of Geosciences, University of Edinburgh, U.K.

11 [4]Key Laboratory for Semi-Arid Climate Change of the Ministry of Education, College of

12 Atmospheric Sciences, Lanzhou University, Lanzhou, China

13 [5]Department of Earth System Science, Tsinghua University, Beijing, China

14 [6]School of Atmospheric Physics, Nanjing University of Information and Technology,

15 Nanjing, China

16 [7]Institute of Urban Meteorology, Chinese Meteorology Administration, Beijing, China

18 Manuscript for submission to *Atmos. Chem. Phys.*

21 *Corresponding authors: Chun Zhao (chunzhao@ustc.edu.cn)

24 Key points:

25 1. Planetary boundary layer (PBL) mixing is the determinant factor in modeling the
26   diurnal cycle of surface PM$_{2.5}$ concentration over East China

27 2. PBL mixing coefficient instead of PBL height is the key factor controlling the simulated
28   diurnal cycle of surface PM$_{2.5}$ concentration in WRF-Chem

29 3. The PBL mixing during the night over East China may be underestimated by WRF-
30   Chem; Increase of PBL mixing during the night can significantly reduce the modeling
31   biases of surface PM$_{2.5}$ concentration and also the modeling sensitivity to the PBL
32   configuration

33 4. The diurnal cycle and injection height of anthropogenic emission have impacts on
34   simulating diurnal cycle of surface PM$_{2.5}$ concentration but smaller than that from PBL
35   mixing

37 **Abstract**

38   Diurnal variation of surface $PM_{2.5}$ concentration (diurnal $PM_{2.5}$) could dramatically affect
39 aerosol radiative and healthy impact, and can also well reflect the physical and chemical
40 mechanisms of air pollution formation and evolution. So far, diurnal $PM_{2.5}$ and its modeling
41 capability over East China have not been investigated, and therefore, are examined in this study.
42 Based on the observations, the normalized diurnal amplitude of surface $PM_{2.5}$ concentrations
43 averaged over East China is the weakest (~1.2) in winter, and reaches ~1.5 in other seasons.
44 The diurnal $PM_{2.5}$ shows the peak concentration during the night in spring and fall and during
45 the daytime in summer. The simulated diurnal $PM_{2.5}$ with WRF-Chem and its contributions
46 from multiple physical and chemical processes are examined in the four seasons. The simulated
47 diurnal $PM_{2.5}$ with WRF-Chem is primarily controlled by planetary boundary layer (PBL)
48 mixing and emission variations, and significantly overestimates the observations during the
49 night. This modeling bias is likely primarily due to the inefficient PBL mixing of primary $PM_{2.5}$
50 during the night. The simulated diurnal $PM_{2.5}$ is sensitive to the PBL schemes and vertical layer
51 configurations with WRF-Chem. The PBL mixing coefficient instead of PBL height is found
52 as the critical factor determining the PBL mixing of pollutants in WRF-Chem. The increase of
53 lower limit of PBL mixing coefficient during the night can significantly reduce the modeling
54 biases in diurnal $PM_{2.5}$ and also the mean concentrations, particularly at the major cities of East
55 China. It can also reduce the modeling sensitivity to the PBL vertical layer configurations. The
56 diurnal variation and injection height of anthropogenic emissions also play roles on simulating
57 diurnal $PM_{2.5}$, but the impact is relatively smaller than that from the PBL mixing. This study
58 underscores that more efforts are needed to improve the boundary mixing process of pollutants
59 in models with observations of PBL structure and mixing fluxes in addition to PBL height, in
60 order to simulate reasonably the diurnal $PM_{2.5}$ over East China. The diurnal variation and
61 injection height of anthropogenic emissions are also necessary to be included to simulate the
62 diurnal $PM_{2.5}$ over East China.

63

64

1. Introduction

The Yangtze River Delta (YRD) region of East China hosts the economic engine and a major portion of the Chinese population. During the past two decades, the rapid economic growth has resulted in significant elevated surface air pollutants over East China, especially particulate matter (PM), also called aerosols. Previous studies have indicated that exposure to the high concentrations of $PM_{2.5}$ (fine particulate matter with aerodynamic diameter less than 2.5 μm) can cause many health issues such as lung cancer (LC), ischemic heart disease(IHD), asthma, and nervous system breakdown (e.g., Seaton A et al., 1995; Davidson C I et al., 2005; Pope III C A et al., 2006; Ho et al., 2018; Li T et al., 2018; Liu T et al., 2018). It has become the fourth risk factor of deaths in China and 11.1% of all deaths are attributable to the ambient elevated concentration of particulate matter (Gakidou et al., 2017). Besides the health impacts, atmospheric aerosol can also influence the radiative energy budget of the Earth's system through interacting with radiation, and serving as cloud condensation nuclei (CCN) and ice nuclei (IN) and hence modifying cloud microphysics (e.g., Ackerman T P., 1977; Dickerson R R et al., 1997; Jacobson M. Z., 1998).

Many studies have investigated spatial and temporal variations of atmospheric aerosol over China in last decades. The $PM_{2.5}$ concentrations are higher in North China than in South China. The highest surface $PM_{2.5}$ concentrations appear in winter and the lowest in summer, and the highest and lowest surface $PM_{2.5}$ concentration of a day often occurs in the evening and afternoon, respectively (e.g., Gong et al., 2007; Fu et al., 2008; Hu et al., 2014; Wang ZF et al., 2014; Wang YG et al., 2014; Wang YJ et al., 2014; Geng et al., 2015; Xie et al., 2015; Zhang and Cao, 2015; Zhang H et al., 2015). Moreover, modeling analysis can help understand the chemical and physical processes affecting aerosol formation and evolution (e.g., Ying et al., 2009; Zhang et al., 2010; Liao et al., 2014; Wang YX et al., 2014; Wang YJ et al., 2014; Hu et al., 2016; Li et al., 2016; Yang et al., 2016; Hu et al., 2017; Zhao B et al., 2017). Yang et al. (2016) reproduced an increasing trend of winter $PM_{2.5}$ concentrations averaged over East China for 1985-2005 with the GEOS-Chem model, and found that the variations in anthropogenic emissions dominated the increase of winter surface $PM_{2.5}$ concentrations over East China and the variations in meteorological fields also played an important role in influencing the decadal increase in winter $PM_{2.5}$ concentrations over East China. Hu et al., (2017) investigated the spatial and temporal distribution of secondary organic aerosol (SOA) in China in 2013 with the WRF-CAMQ model and found that the formation of SOA from biogenic emissions was significantly enhanced due to anthropogenic emissions.

98   Most of previous modeling studies focused on understanding the mechanisms driving PM

99   variation on daily or seasonal scales or/and evaluating the simulation of daily and monthly

100   mean PM concentrations over East China. Few studies evaluated the model performance in

101   simulating diurnal cycle of surface PM concentration and investigated the mechanisms

102   underneath. However, the model capability of capturing diurnal cycle of surface PM

103   concentration is critical for revealing mechanisms of PM formation and evolution and may also

104   affect simulating mean concentration. Some studies also found that diurnal variation of surface

105   PM concentration can affect the daily average radiative forcing (e.g., Arola A et al., 2013;

106   Kassianov E et al., 2013; Kuang Y et al., 2015; Wang Z et al., 2015; Song et al., 2018). Based

107   on the ground-based data collected in Hefei from 2007 to 2013, Wang Z et al. (2015)

108   demonstrated that using daily averaged aerosol properties to retrieve the 24-h average direct

109   aerosol radiative forcing can have positive biases of up to 7.5 W m^{-2} for the cases. Arola et al.

110   (2013) found that the aerosol optical depth (AOD) diurnal cycles have significant impacts on

111   the daily mean aerosol radiative forcing.

112   Previous studies have observed evident diurnal variations of surface PM over East China

113   (e.g., Gong et al., 2007; Gu et al., 2010; Pathak R K et al., 2011; Feng et al., 2014; Hu et al.,

114   2014; Huang et al., 2014; Ma et al., 2014; Zhang and Cao, 2015; Chen et al., 2016; Tao et al.,

115   2016; Zhao et al., 2016; Chen et al., 2017; Jia et al., 2017; Guo H et al., 2017; Guo J et al.,

116   2017;). Zhang and Cao (2015) used a long-term dataset of surface $PM_{2.5}$ concentration

117   measured at 190 cities of China, and found that the diurnal variation of the $PM_{2.5}$-to-CO ratio

118   consistently displayed a pronounced peak during the afternoon, reflecting a significant

119   contribution of secondary PM formation. Guo H et al. (2017) investigated the diurnal cycle of

120    $PM_{2.5}$ in China with the observations obtained at 226 sites of China during the period of January

121   of 2013 to December of 2015 and found the surface $PM_{2.5}$ concentration reached the maximum

122   in the morning over the YRD region.

123   Diurnal variation of surface PM concentration can be controlled by many factors including

124   emissions, chemical reactions, and meteorology (e.g., Wang et al., 2006; Huang et al., 2010;

125   Wang et al., 2010; Menut et al., 2012; Qi et al., 2012; Quan et al., 2013; Tiwari et al., 2013; Li

126   et al., 2014; Pal et al., 2014; Sun et al., 2015; Zhang and Cao, 2015; RR Rodelas et al., 2019;

127   Xu et al., 2019). Wang et al. (2010) found that simulations with hourly emission inventory can

128   reproduce the diurnal variation patterns and magnitude of AOD better than simulations with

129   daily emission inventory. Xu et al. (2019) compared the diurnal cycles of aerosol species

130   between 2014 and 2016 observed by Aerodyne high‑resolution aerosol mass spectrometer in

131   Beijing and found that the increase of secondary inorganic nitrate, sulfate, and ammonium

132   throughout the day in 2016 were mainly caused by the enhanced photochemical production.

133   With the dataset of PBL height derived from the space-borne and ground-based lidar, Su et al.

134   (2018) investigated the relationship between PBL height and surface PM concentrations across

135   China and found nonlinearly negative responses of PM to PBL height evolution over polluted

136   regions, especially when the PBL height is shallow and PM concentration is high.

137   Since very few studies evaluated the modeling performance of diurnal cycle of surface

138   PM concentration over East China and investigated the mechanisms underneath, this study

139   investigates the WRF-Chem (Weather Research and Forecasting model coupled with

140   Chemistry) simulation of diurnal variation of $PM_{2.5}$ over East China. WRF-Chem (Grell et al.,

141   2005) is an online-coupled meteorology and chemistry model that simulates meteorological

142   fields and air pollutant concentrations simultaneously. It has been widely used for studying the

143   temporal and spatial variation of aerosols (e.g., Jiang et al., 2012; Zhou et al., 2014; Bei et al.,

144   2016; Wang et al., 2016; Zhang et al., 2016; Zhong et al., 2016; Li et al., 2017; Zhao et al.,

145   2017; Zhou et al., 2017; Liu S et al., 2018; Ni et al., 2018) and their meteorological and climatic

146   impacts over East China (e.g., Gong et al., 2007; Ding et al., 2013; Wu et al., 2013; Gao et al.,

147   2014; Chen et al., 2014; Zhao et al., 2014; Zhang B et al., 2015; Zhang L et al., 2015; Huang

148   et al., 2016; Liu et al., 2016; Petäjä et al., 2016; Zhao B et al., 2017). Most of the previous

149   modeling studies with WRF-Chem over China investigated the influencing factors on spatial

150   distribution and monthly or seasonal variation of PM. None of them focused on the

151   performance of simulating diurnal variation of PM with WRF-Chem.

152   The study will examine the observed characteristics of diurnal variation of surface $PM_{2.5}$

153   concentration over the YRD region of East China in four seasons of 2018. The WRF-Chem

154   simulations are conducted for one month of each season over East China as shown in Fig 1a,

155   and the simulated diurnal cycle of surface $PM_{2.5}$ concentration will be evaluated through

156   comparing with hourly observations of surface $PM_{2.5}$ concentration released by the Ministry of

157   Environmental Protection (MEP) of China for 190 stations over the YRD region of East China

158   in 2018. The model is also used to investigate the mechanisms driving the diurnal cycle of

159   surface $PM_{2.5}$. This study will focus on the impacts from meteorology and anthropogenic

160   emissions on the diurnal variation of surface $PM_{2.5}$ concentration. For meteorology, we will

161   focus on the PBL mixing process that has been found largely controlling the diurnal variation

162   of surface pollutant concentrations (Liu M et al., 2018). For emissions, based on the findings

163   of Wang et al. (2010) and Yang et al. (2019), the diurnal variation and injection height of

164   emission will be investigated. The rest of the paper is organized as follows. The detailed

165   introduction of WRF-Chem model and numerical experiments, anthropogenic emissions, and

166   observations will be presented in Section 2. The examination of simulated diurnal variation of

167   surface $PM_{2.5}$ concentrations and the impacts of PBL mixing and emission will be discussed in

168   Section 3. The conclusions can be found in Section 4.

169

170   **2. Methodology**

171   **2.1 Models and experiments**

172   2.1.1 WRF-Chem

173   In this study, the version of WRF-Chem updated by University of Science and Technology

174   of China (USTC version of WRF-Chem) is used. This USTC version of WRF-Chem includes

175   some additional capabilities such as the diagnosis of radiative forcing of aerosol species, land

176   surface coupled biogenic VOC emission, aerosol-snow interaction compared with the

177   publically released version (Zhao et al., 2013a,b, 2014, 2016; Hu et al., 2019). Particularly, in

178   order to understand the modeling mechanisms driving the diurnal variations of surface $PM_{2.5}$

179   concentration over East China, this study updates the USTC version of WRF-Chem to include

180   the diagnosis of contribution to surface $PM_{2.5}$ concentration from individual process including

181   transport, emission, dry and wet deposition, PBL mixing, and chemical production/loss through

182   estimating the difference of surface $PM_{2.5}$ concentration before and after individual process

183   during the simulation.

184   The Model for Simulating Aerosol Interactions and Chemistry (MOSAIC, Zaveri and

185   Peter,1999; Zaveri et al.,2008) and the CBM-Z (carbon bond mechanism) photochemical

186   mechanism (Zaveri and Peters, 1999) are used. The MOSAIC aerosol scheme includes physical

187   and chemical processes of nucleation, condensation, coagulation, aqueous phase chemistry,

188   and water uptake by aerosols. All major aerosol components including sulfate, nitrate,

189   ammonium, black carbon, organic matter, sea salt, mineral dust, and other inorganics (OIN)

190   are simulated in the model. Aerosol size distributions are represented by eight discrete size bins

191   through the bin approach (Fast et al., 2006). Dry deposition of aerosol mass and number is

192   simulated following the approach of Binkowski and Shankar (1995), which includes both

193   particle diffusion and gravitational effects. Wet removal of aerosols by grid resolved stratiform

194   clouds/precipitation includes in-cloud removal (rainout) and below-cloud removal (washout)

195   by impaction and interception, following Easter et al. (2004) and Chapman et al. (2009). In this

196   study, cloud-ice-borne aerosols are not explicitly treated in the model but the removal of

197   aerosols by the droplet freezing process is considered. Convective transport and wet removal

198   of aerosols by cumulus clouds follow Zhao et al. (2013a). Aerosol radiative feedback is coupled

199   with the Rapid Radiative Transfer Model (RRTMG) (Mlawer et al., 1997; Lacono et al., 2000)

200   for both SW and LW radiation as implemented by Zhao et al. (2011). The optical properties

201   and direct radiative forcing of individual aerosol species in the atmosphere are diagnosed

202   following the methodology described in Zhao et al. (2013b). A detailed description of the

203   computation of aerosol optical properties in WRF-Chem can be found in Fast et al. (2006) and

204   Barnard et al. (2010). Aerosol-cloud interactions were included in the model by Gustafson et

205   al. (2007) for calculating the activation and re-suspension between dry aerosols and cloud

206   droplets.

207

208   2.1.2 Numerical experiments

209   In this study, WRF-Chem is conducted with two nested domains (one-way nesting) in one

210   month of each season of 2018 (i.e., January, April, July, October of 2018). The outer quasi-

211   global domain with 360×145 grid cells (180 °W~180 °E,67.5 °S~77.5 °N) at the 1 °×1 °horizontal

212   resolution is used to provide the chemical boundary to the inner domain with 112×105 grid

213   cells (109.0 °E~124.9 °E, 24.0 °N~38.9 °N) at the horizontal resolution of 15 km over East China

214   covering the entire YRD region as shown in Figure 1a. More details about the quasi-global

215   WRF-Chem simulation can be found in Zhao et al. (2013a) and Hu et al. (2016). To better

216   resolve the PBL structure and mixing and examine the modeling sensitivity to vertical

217   configuration within PBL, two experiments (CTL1 and CTL2, Table 1) are configured with 40

218   vertical layers but have different distributions (as shown Fig. 1b). One configuration (L1) has

219   roughly 20 layers below 2 km above the ground, and the other has about 10 layers below 2 km

220   (Fig. 1b). In both CTL1 and CTL2, MYNN2 PBL scheme (Nakanishi and Niino, 2006) is used.

221   To demonstrate the modeling sensitivity to PBL parameterizations, the experiment CTL3 is

222   conducted as the way similar to CTL2 but with the YSU PBL scheme (Hong et al., 2006). Two

223   additional sensitivity experiments (EXP1 and EXP2, Table 1) are also conducted

224   corresponding to the experiments CTL1 and CTL2, respectively, except that the PBL mixing

225   coefficient is modified (see details in Section 3.2.2). All these WRF-Chem experiments use the

226   Morrison two-moment cloud microphysics (Morrison et al., 2009), Kain-Fritsch convective

227   scheme (Kain et al., 2004), CLM land surface scheme, and RRTMG longwave and shortwave

228   radiation schemes. The meteorological initial and lateral boundary conditions are derived from

229   the NCEP Final reanalysis data with 1 °×1 °degree resolution and 6-hour temporal resolution.

230   The modeled u component and v component wind and atmospheric temperature are nudged

231   towards the reanalysis data only to the layers above the PBL with nudging coefficients of 3×10^{-4} s^{-1} with a nudging timescale of 6-hour (Stauffer and Seaman, 1990; Seaman et al., 1995).

232

233

234   2.1.3 Emissions

235   Anthropogenic emissions for the outer quasi-global simulation are obtained from the

236   Hemispheric Transport of Air Pollution version-2 (HTAPv2) at $0.1°\times0.1°$ horizontal resolution

237   and a monthly temporal resolution for year 2010 (Janssens-Maenhout et al., 2015), except that

238   emissions over China within the domains are from the Multi-resolution Emission Inventory for

239   China (MEIC) at $0.1°\times0.1°$ horizontal resolution for 2015 (Li M et al., 2017), which is also

240   used for the inner domain simulation over East China. Figure 1a shows the spatial distributions

241   of emissions of primary $PM_{2.5}$, NO_x, and SO_2 over East China. The default anthropogenic

242   emission inventories assume no diurnal variation of emissions and that all emissions are near

243   the surface (e.g., first model layer). Since diurnal variation of emissions and injection height

244   of power plant emissions may have impacts on diurnal variation of surface pollutants, the

245   experiments discussed above apply the diurnal profiles of anthropogenic emissions from five

246   individual sector (i.e., agriculture, industry, transport, energy, and residential) following

247   Olivier et al. (2003) and Wang et al. (2005) as shown in Fig. 1c and vertical distributions of

248   anthropogenic power plant emissions following Wang et al. (2010) as shown in Table 2. As

249   shown in Fig. 1c, emissions from all sectors show peak values during the daytime, and the

250   diurnal variations from agriculture, residential, and transportation are much stronger than those

251   from industry and power plant. The emissions from power plant are distributed from the bottom

252   to a height of ~900 m with more than 90% below 500 m. Two sensitivity experiments,

253   EXP1_E1 and EXP1_E2, are conducted as the way similar to EXP1 except that EXP1_E1

254   assumes no diurnal variation of anthropogenic emissions and EXP1_E2 assumes all power

255   plant emissions are placed near the surface (i.e., the first model layer). Comparing EXP1 with

256   EXP1_E1 and EXP1_E2 can examine the impact of diurnal variation and injection height of

257   anthropogenic emissions on diurnal cycle of surface $PM_{2.5}$, respectively. All these experiments

258   are summarized in Table 1. Biomass burning emissions are obtained from the Fire Inventory

259   from NCAR (FINN) with hourly temporal resolution and 1 km horizontal resolution

260   (Wiedinmyer et al., 2011), and are vertically distributed following the injection heights

261   suggested by Dentener et al. (2006) from the Aerosol Comparison between Observations and

262   Models (AeroCom) project. Sea-salt emission follows Zhao et al. (2013a), which includes

263   correction of particles with radius less than 0.2 μm (Gong, 2003) and dependence of sea-salt

264   emission on sea surface temperature (Jaeglé et al., 2011). The vertical dust fluxes are calculated

265   with the GOCART dust emission scheme (Ginoux et al., 2001), and the emitted dust particles

266   are distributed into the MOSAIC aerosol size bins following a theoretical expression based on

267   the physics of scale-invariant fragmentation of brittle materials derived by Kok (2011). More

268   details about the dust emission scheme coupled with MOSAIC aerosol scheme in WRF-Chem

269   can be found in Zhao et al. (2010, 2013a).

270

271   **2.2 Observations**

272   The ground observations of hourly surface $PM_{2.5}$ mass concentration in January, April,

273   July, and October of 2018 are obtained from the website of the Ministry of Environmental

274   Protection of China (MEP of China). Since this study focuses on the YRD region of East China,

275   190 stations over East China are selected for analysis. The locations of these 190 stations are

276   shown in Fig. 1a within the black box (116.0 °E~122.5 °E,29.0 °N~33.0 °N). Besides regional

277   average analysis, four cities (Fig. 1a) as the Center (Shanghai, 121.45 °E and 31.21 °N) and sub-

278   Center (Nanjing, 118.78 °E and 32.06 °N; Hefei, 117.25 °E and 31.85 °N; Hangzhou, 120.08 °E

279   and 30.21 °N) of the YRD city cluster are also selected for further analysis at urban areas.

280

281   **3. Results**

282   **3.1 Modeling diurnal cycle of surface $PM_{2.5}$ concentration**

283   In order to investigate the diurnal cycle of surface $PM_{2.5}$ concentration, this study defines

284   an index to better show the diurnal variation. The diurnal index (DI) is defined as the value of

285   each hour divided by the minimum value within 24-hour on monthly average. The peak DI

286   within 24-hour represents the amplitude of diurnal variation. Figure 2 shows the diurnal index

287   of surface $PM_{2.5}$ concentration within 24-hour averaged over the YRD region of East China (as

288   shown as the black box in Fig. 1a) for January, April, July, October of 2018 from the WRF-

289   Chem experiments and observations. The experiment CTL1 uses the MYNN PBL scheme and

290   finer boundary layer configuration (L1 in Fig. 1b). The simulation results are 3-hourly and

291   sampled at the observational sites as shown in Fig. 1a. On regional average, the observed

292   variation of DI is the weakest in winter with the peak value around 1.2 among the four seasons.

293   The observed DI reaches the maximum of 1.5 in autumn. In spring and autumn, the observed

294   diurnal variation of DI is similar, showing two peaks in the morning and night, respectively,

295   and reaching the minimum in the afternoon, which is consistent with previous findings with

296   observations over East China (e.g., Zhang and Cao., 2015; Liu et al.,2016; Guo et al.,2017). In

297   summer, different from other seasons, the observed diurnal variation of DI shows the single

298   peak around 1.4 near the noon time. The CTL1 experiment can generally reproduce two peaks

299   in spring and autumn, however, the CTL1 simulation overestimates the observed peak DI in

300   the two seasons, particularly in autumn. The experiment generally captures the seasonality of

301   DI of surface $PM_{2.5}$ concentration that is higher DI in spring and autumn and the weakest DI in

302   winter, except that in summer the experiment significantly overestimates the DI during the

303   night and produces opposite diurnal pattern with the minimum DI near the noon time. The

304   spatial distributions of DI over East China are also generally consistent between observations

305   and simulations and show similar seasonality (Figure S1 in the supporting material). The area

306   with higher surface $PM_{2.5}$ concentration generally has higher DI (Figure S2 in the supporting

307   material), particularly from the simulation.

308   Therefore, the DI distribution at the four cities as the Center (Shanghai) and sub-Center

309   (Nanjing, Hefei, Hangzhou) of the YRD city cluster in East China (as shown in Fig. 1a) are

310   further analyzed. Figure 3 shows the diurnal index of surface $PM_{2.5}$ concentration within 24-

311   hour averaged over the four cities for January, April, July, October of 2018 from the WRF-

312   Chem experiments and observations. The observed diurnal variation of DI in these four cities

313   are consistent with that on regional average of East China. The diurnal variation of DI is more

314   evident in the two inland cities (Hefei and Nanjing) than the two coastal cities (Hangzhou and

315   Shanghai). Consistent with the results based on regional average, the CTL1 experiment can

316   generally capture the diurnal variation of DI of surface $PM_{2.5}$ in the four cities, but

317   overestimates the DI in the night, particularly in spring and autumn. In summer, again, the

318   CTL1 significantly overestimates the DI during the night and produces the opposite diurnal

319   pattern compared to observations. In general, the CTL1 produces even higher DI during the

320   night in the four cities than regional average, which results in larger diurnal amplitudes in the

321   four cities than regional average. The CTL1 can generally simulate stronger diurnal variation

322   in the two inland cities than in the two coastal cities.

323   The analysis above for both regional average and city average indicates that the CTL1

324   simulation has high positive biases of DI during the night. In order to understand the modeling

325   biases and the mechanisms driving the simulated diurnal variations of surface $PM_{2.5}$

326   concentration over East China, the contribution to diurnal variation of surface $PM_{2.5}$

327   concentration from individual process including transport, emission, dry and wet deposition,

328   mixing, and chemical production/loss is estimated. The contribution is calculated as the

329   difference of surface $PM_{2.5}$ concentration before and after individual process during the

330   simulation. Figure 4 shows the contribution of individual process to the variation of surface

331   PM$_{2.5}$ concentration every 3-hour in Hefei from the WRF-Chem experiments averaged for

332   January, April, July, and October of 2018. The 3-hourly tendency of surface PM$_{2.5}$

333   concentration is also shown. The contributions and tendencies are divided by monthly mean

334   surface PM$_{2.5}$ concentration for each month. The results for the other three cities (Nanjing,

335   Hangzhou, Shanghai) are similar to that of Hefei and are shown in the supporting material

336   (Figure S3a-c). Process contribution analysis is verified by comparing the variations of surface

337   PM$_{2.5}$ concentration with the sum of the contribution from each individual process. As shown

338   in Figure S4, the sum contributions of all processes are consistent with the variations in surface

339   PM$_{2.5}$ concentration following the principle of mass balance.

340   In Fig. 4, positive value denotes relative increase of surface PM$_{2.5}$ concentration and

341   negative value denotes relative decrease. From the CTL1 experiment, the contributions from

342   emission and chemistry are positive through the day, while the contributions from transport,

343   PBL mixing, wet and dry deposition are negative through the day. The CTL1 simulates the

344   largest variation of tendency in summer and the smallest variation in winter. The tendency is

345   negative from the morning to the afternoon, resulting the simulated minimum surface PM$_{2.5}$

346   concentration in the afternoon in all seasons, which is consistent with the result shown in Fig.

347   3. It is evident that emission, PBL mixing, and transport are the three main processes

348   controlling the diurnal variation of surface PM$_{2.5}$ concentration, and emission and PBL mixing

349   are the dominant two. Emission increases the surface PM$_{2.5}$ concentration and reaches the

350   maximum near the noon time, while PBL mixing reduces the surface PM$_{2.5}$ concentration and

351   also reaches the maximum reduction near the noon time. The combined effect of emission and

352   PBL mixing is reflected as the overall tendency. Therefore, PBL mixing is the determinant

353   process leading to the simulated minimum DI near the noon time and higher DI during the

354   night. To further demonstrate the contribution of each PM$_{2.5}$ composition to the diurnal

355   variation of surface PM$_{2.5}$ concentration, Figure 5 shows the diurnal variation of surface

356   concentration of each PM$_{2.5}$ composition in Hefei from the WRF-Chem experiments averaged

357   for January, April, July, and October of 2018. The diurnal variations of surface concentrations

358   of OM, BC, and OIN are larger than other components of PM$_{2.5}$, showing evident higher

359   concentration during the night and minimum near the noon time in all seasons except winter.

360   The sum of OM and OIN contribute to more than half of surface PM$_{2.5}$ concentration. Therefore,

361   it suggests that the PBL mixing of the primary PM$_{2.5}$ determines the simulated diurnal variation

362   of surface PM$_{2.5}$ concentration. The results for the other three cities (Nanjing, Hangzhou,

363   Shanghai) are similar to that of Hefei and are shown in the supporting material (Figure S5a-c).

364

3.2 Sensitivity to PBL mixing

3.2.1 Sensitivity to the PBL configuration

As discussed above, the PBL mixing is very important for modeling diurnal variation of surface $PM_{2.5}$ concentration, and it may be affected by PBL parameterizations and vertical layer configuration within the PBL. Therefore, two experiments, CTL2 and CTL3, are conducted to examine the sensitivity of simulated diurnal variation of surface $PM_{2.5}$ concentration to different PBL configurations. The CTL2 uses the MYNN PBL scheme as the CTL1 but is configured with different vertical layer distribution (L2) as shown in Fig. 1b, in which less vertical layers are put within the PBL as described in Section 2.2. The CTL3 uses the YSU PBL scheme and is configured with the L2 vertical layer distribution as the CTL2. As shown in Fig. 2, on regional average, the CTL2 and CTL3 generally simulate similar diurnal and seasonal patterns as that by the CTL1 with the minimum DI near the noon time and the peak DI during the night. The CTL2 simulates lower DI than the CTL1 during the night in all seasons. This indicates that the model with finer vertical resolution within the PBL, which is supposed to better resolve the PBL structure, produces higher positive biases of DI. The CTL3 simulates similar diurnal variation of DI as the CTL2 but overestimate the DI during the night to some extent, particularly in summer, which indicates the model with the YSU PBL scheme produces higher positive biases of DI during the night compared to the one with the MYNN PBL scheme. In the four cities as shown in Fig. 3, the CTL2 and CTL3 also simulate similar diurnal and seasonal patterns as that by the CTL1. It is also interesting to note that the difference of DI between CTL2 and CTL1 are larger than that between CTL3 and CTL2, which indicate that the modeling sensitivity of DI to the vertical layer configuration within the PBL is even greater than that to the PBL scheme. Overall, all these three WRF-Chem experiments produce similar positive biases of DI during the night compared to the observations in all seasons over the YRD region of East China, particularly in cities. This is consistent with previous findings about the simulated positive biases of diurnal variation of surface $PM_{2.5}$ concentration over East China (e.g., Liu M et al., 2018). The changes of PBL schemes and vertical configurations within the PBL can affect the simulated DI but cannot improve the simulations to reproduce the observations.

In order to better understand the modeling sensitivity of DI to the PBL configuration, Fig. 4 and 5 also shows the simulated results for the city of Hefei from the CTL2 and CTL3. Similar as CTL1, the results from CTL2 and CTL3 also show that emission, PBL mixing, and transport are the three main processes controlling the diurnal variation of surface $PM_{2.5}$ concentration, and emission and PBL mixing are the dominant two (Fig. 4). Since the number

399   of vertical layer within the PBL in CTL2 and CTL3 is much less than that in CTL1, the

400   thickness of first model layer in CTL2 and CTL3 is about a factor 2 of that in CTL1. With the

401   same emission flux, CTL2 and CTL3 simulate much smaller contribution from emission to the

402   surface $PM_{2.5}$ concentration than does CTL1. Correspondingly, the contribution from PBL

403   mixing to the surface $PM_{2.5}$ concentration in CTL2 and CTL3 is also lower than that in CTL1.

404   The combined effect of emission and PBL mixing results in weaker diurnal variation of surface

405    $PM_{2.5}$ concentration in CTL2 and CTL3 than that in CTL1, as shown by the diurnal variation

406   of overall tendency of surface $PM_{2.5}$ concentration. CTL3 with the YSU PBL scheme simulates

407   stronger diurnal variation of surface $PM_{2.5}$ concentration than does the CTL2 with the MYNN

408   PBL scheme, primarily due to its larger diurnal variation of PBL mixing. With less contribution

409   from emission to the surface $PM_{2.5}$ concentration, CTL2 and CTL3 simulate less primary $PM_{2.5}$

410   (OIN, OM, BC) than does CTL1 (Fig. 5), particularly during the night when the PBL mixing

411   is weak. This leads to the weaker diurnal variation of total surface $PM_{2.5}$ concentration in CTL2

412   and CTL3 as discussed above. The higher DI during the night in CTL3 than CTL2 can also be

413   explained by the higher primary $PM_{2.5}$ during the night due to weaker PBL mixing.

414

415   3.2.2 Sensitivity to the PBL mixing coefficient

416   The results discussed above suggest that, the WRF-Chem simulated diurnal variation of

417   surface $PM_{2.5}$ concentration over East China is largely controlled by the PBL mixing process,

418   and is sensitive to the PBL scheme and vertical layer configuration within the PBL. However,

419   the increase of number of vertical layer within the PBL and use of different PBL schemes

420   cannot reduce the modeling biases in diurnal variation of surface $PM_{2.5}$ concentration. Many

421   previous studies investigated the PBL mixing of pollutants through establishing the

422   relationship between surface pollutant concentration and PBL height. However, it is

423   noteworthy that in most atmospheric models, the mixing of pollutants within the PBL is treated

424   either as full mixing within the PBL height (i.e., uniformly distributed within the PBL height)

425   or as calculated based on the mixing coefficient diagnosed from the PBL scheme. The former

426   method represents the strongest PBL mixing and the surface concentration can be largely

427   influenced by the PBL height. However, the latter one means that the pollutant mixing does

428   not depend explicitly on PBL height.

429   In WRF-Chem, the PBL mixing of pollutants is treated with the second approach. In order

430   to further examine the simulated PBL mixing process in this study, Figure 6 shows the diurnal

431   variation of PBL heights and PBL mixing coefficients below PBL height in Hefei in January,

432   April, July, and October of 2018 from the WRF-Chem experiments CTL1, CTL2, and CTL3.

433   The black line represents the PBL height while the contour shading represents the PBL mixing
434   coefficients within the PBL height. First of all, the PBL heights simulated from the three
435   experiments all show evident diurnal variation with the maximum in the daytime and the
436   minimum during the night. The simulated PBL heights from CTL1 and CTL2 with the same
437   PBL scheme (MYNN) show very similar diurnal pattern, indicating the vertical layer
438   configuration has small impact on modeling PBL height. Both experiments simulate the largest
439   diurnal variation of PBL height in summer with a changing factor of ~10 from ~2 km in the
440   afternoon to ~200 m in the early morning, and the smallest diurnal variation of PBL height in
441   winter with a changing factor of 2 from ~700 m in the afternoon to ~350 m in the early morning.
442   It should be noted that the PBL mixing coefficients within the PBL also exhibit evident diurnal
443   variation with a changing factor of ~1000 and ~50 in summer and winter, respectively, which
444   is much larger than that of the PBL height in all seasons. The CTL3 simulation with the YSU
445   PBL scheme also show that the diurnal variation of PBL mixing coefficient is much larger than
446   that of PBL height. The difference between CTL2 and CTL3 is consistent with the analysis
447   about the simulated diurnal variation of surface $PM_{2.5}$ concentration, further demonstrating that
448   the WRF-Chem simulated diurnal variation of surface $PM_{2.5}$ concentration is determined by
449   the PBL mixing coefficient instead of PBL height. For example, in autumn the PBL height
450   during the night is lower in CTL3 than in CTL2, while the DI during the night is lower in CTL3
451   than in CLT2 (Fig. 3) due to the higher PBL mixing coefficient during the night in CTL3 than
452   in CTL2. More WRF experiments with different PBL schemes are conducted and all show
453   similar results that the diurnal variation of PBL mixing coefficient is much stronger than that
454   of PBL height (not shown).

455   With relatively large values of PBL mixing coefficient during the daytime, the emitted
456   pollutants can be mixed up roughly reaching the layer of PBL height. However, weak PBL
457   mixing coefficient during the night results in that the emitted $PM_{2.5}$ and its precursors will stay
458   near the surface (i.e., within the first layer of model) during the night and cannot be mixed up
459   reaching the PBL height (Fig. S6 in the supporting material). This leads to the large difference
460   of DI between CTL1 and CTL2 with different thickness of first model layer during the night
461   although they simulate similar PBL height. The comparison between simulations and
462   observations (Fig. 2 and 3) suggests the positive modeling biases of DI during the night may
463   be partly due to the underestimation of the PBL mixing during the night. To examine the
464   sensitivity of simulated DI to the PBL mixing coefficient, the sensitivity experiments, EXP1
465   and EXP2, are conducted corresponding to CTL1 and CTL2, respectively, through setting the
466   lower limit of PBL mixing coefficient from 0.1 m²/s (default in the publically released version

467   of WRF-Chem) to 5 m^2/s within the PBL. Figure 7 shows the simulated PBL height and mixing

468   coefficients from the two sensitivity experiments, EXP1 and EXP2, in January, April, July, and

469   October of 2018 in Hefei. It shows that the PBL mixing coefficient increases during the night

470   within the PBL compared to the results shown in Fig. 6, while the values during the daytime

471   remain almost the same. The difference of simulated surface $PM_{2.5}$ between CTL1 and EXP1

472   is relatively small during the daytime, but significant during the night, which is due to that

473   EXP1 can mix up the surface $PM_{2.5}$ to the PBL height during the night (Fig. S6). It is

474   noteworthy that the lower limit parameter of 5 m^2/s is entirely empirical. It is selected to

475   represent the moderate mixing strength between the full PBL mixing and no PBL mixing. A

476   few other values such as 1 m^2/s and 10 m^2/s are also tested. The results do not change the

477   conclusion found in this study and therefore are not shown.

478   The change of PBL mixing coefficient during the night can significantly affect the diurnal

479   variation of PBL mixing. Figure 8 shows the contribution of individual process to the variation

480   of surface $PM_{2.5}$ concentration every 3-hour in Hefei simulated by EXP1 and EXP2 averaged

481   for January, April, July, and October of 2018. The 3-hourly tendency of surface $PM_{2.5}$

482   concentration is also shown. Same as Fig. 4, the contributions and tendencies are divided by

483   monthly mean surface $PM_{2.5}$ concentration for each month. The results for the other three cities

484   (Nanjing, Hangzhou, Shanghai) are similar to that of Hefei and are shown in the supporting

485   material (Figure S7a-c). Compared to the results from CTL1 and CTL2 shown in Fig. 4, it is

486   evident that the diurnal variation of tendency of surface $PM_{2.5}$ concentration is significantly

487   reduced in all seasons. This is mainly resulted from the significantly reduced diurnal variation

488   of PBL mixing contribution. Specifically, the PBL mixing contribution during the night is

489   increased. Figure 9 shows the diurnal variation of surface concentration of each $PM_{2.5}$

490   composition in Hefei simulated by the EXP1 and EXP2 averaged for January, April, July, and

491   October of 2018. The diurnal variations of surface concentrations of OM, BC, and OIN are

492   significantly reduced primarily due to their reduced concentration during the night in EXP1

493   and EXP2, compared to CTL1 and CTL2 (Fig. 5). The results for the other three cities (Nanjing,

494   Hangzhou, Shanghai) are similar to that of Hefei and are shown in the supporting material

495   (Figure S8a-c).

496   The change of PBL mixing and diurnal variation of primary $PM_{2.5}$ near the surface turn

497   out different DI. Figure 10 shows the diurnal variation of DI of surface $PM_{2.5}$ averaged over

498   the YRD region of East China for January, April, July, and October of 2018 from the

499   observations and the experiments CTL1, CTL2, EXP1, and EXP2. In general, the simulated

500   DI are reduced significantly during the night in EXP1 and EXP2 much more consistent with

501   the observations compared to the ones in CTL1 and CTL2. In spring, the EXP1 and EXP2
502   slightly underestimate DI during night. Figure 11 shows the diurnal variation of DI averaged
503   over the four cities for January, April, July, October of 2018 from the observations and the
504   experiments CTL1, CTL2, EXP1, and EXP2. As discussed above the diurnal variation of DI is
505   much stronger in cities with relatively more emissions. The simulated DI is also more sensitive
506   to the change of PBL mixing coefficient in these four cities compared to that on regional
507   average. The EXP1 and EXP2 produce much more consistent DI with the observations in the
508   four cities than do CTL1 and CTL2 in all seasons. It is also noteworthy that the difference
509   between EXP1 and EXP2 and that between CTL1 and CTL2 is reduced both on city average
510   and regional average, which indicates that the enhanced PBL exchange coefficient during the
511   night help reduce the modeling sensitivity to the vertical layer configuration. The analysis
512   above suggests that the simulated PBL mixing during the night in the publically-released WRF-
513   Chem may be too weak.

514   Comparing the simulated surface concentrations of $PM_{2.5}$ components between CTL1 (Fig.
515   5) and EXP1 (Fig. 9), it can be found that the daily average surface $PM_{2.5}$ mass concentration
516   should also be reduced when the diurnal variation is reduced due to the reduction of nighttime
517   surface $PM_{2.5}$ concentration. Figure 12 shows the comparison of monthly mean surface $PM_{2.5}$
518   concentration between the observations and the simulations from CTL1 and EXP1 at each
519   observation site over the YRD region of East China for January, April, July, and October of
520   2018. In all seasons, the CTL1 significantly overestimates the observed surface $PM_{2.5}$
521   concentration with the normalized mean biases (NMB) of 22% (winter) - 109% (summer) on
522   regional average. The EXP1 reduces the NMB to 7% (winter) - 38% (summer) on regional
523   average. In CTL1, the NMB of simulation exceeds 50% at 20%, 35%, 65%, and 60% of
524   observational sites over the YRD region of East China in January, April, July, and October,
525   respectively, which reduces to 0%, 10%, 35%, and 20% of all sites in EXP1. In addition, the
526   EXP1 also increases the spatial correlation between observations and simulated results in all
527   seasons (Fig. 12), although with the improvement of modeling diurnal variation the EXP1 still
528   cannot fully capture the observed spatial variability of surface $PM_{2.5}$ concentration among the
529   observational sites. This may be related to the biases in spatial distributions of emission and
530   model processes contributed to the spatial variability of surface $PM_{2.5}$ concentration, which
531   deserves further investigation in future.
532
533   **3.3 Impacts from emission distributions**
534   3.3.1 Impacts from emission diurnal variability

535   Besides the meteorology such as PBL mixing as discussed above, the diurnal variation of

536   emissions may also play an important role in determining the DI of surface $PM_{2.5}$ concentration.

537   One sensitivity experiment, EXP1_E1, without diurnal variation of anthropogenic emissions

538   (Fig. 1b) is conducted. Figure 13 shows the spatial distribution of the difference in maximum

539   DI between EXP1 and EXP1_E1 over East China. As removing diurnal variation of emissions

540   will lead to more emissions during the night and thus increase the DI during the night over

541   polluted area, which generally results in larger maximum DI. Therefore, EXP1 has lower

542   maximum DI than EXP1_E1 over most regions of East China in seasons other than winter.

543   EXP1 could have slightly larger maximum DI in winter when the diurnal variation of DI is

544   relatively small (Fig. 2 and 3) and over the relatively clean region (Fig. 1a) in summer. Figure

545   14 shows the diurnal index of surface $PM_{2.5}$ concentration within 24-hour averaged over the

546   four cities for January, April, July, and October of 2018 from observations and the EXP1 and

547   EXP1_E1 experiments. In general, EXP1 shows lower DI than EXP1_E1 during the night, and

548   therefore has smaller diurnal variation of DI in four cities. The largest difference between EXP1

549   and EXP1_E1 in four cities exists in summer and the smallest is in winter. Comparing to the

550   impacts from PBL mixing as shown in Fig. 11, the reduction of diurnal variation of DI by

551   adding diurnal variation of anthropogenic emissions is much smaller.

552   Fig. 13 shows that EXP1 with diurnal variation of emissions could simulate slightly larger

553   diurnal variation of DI over the relatively clean region than EXP1_E1 in winter and summer.

554   The higher DI in EXP1 than EXP1_E1 is primarily in the afternoon and evening (Fig. S9 in

555   the supporting material). One grid over south Anhui is selected for analysis of contributions

556   from different processes in the model to the diurnal variation of surface $PM_{2.5}$ concentration

557   from the experiments EXP1 and EXP1_E1 (Fig. 15). Different from the process contributions

558   over the relatively polluted region (Fig. 8), the contribution from direct local emission to the

559   surface $PM_{2.5}$ concentration is relatively small over the clean region. Instead, the contributions

560   from chemistry, dry deposition, PBL mixing, and transport dominate the diurnal variation of

561   surface $PM_{2.5}$ concentration. The PBL mixing could increase the surface $PM_{2.5}$ concentration

562   during the daytime because of mixing down the pollutants transported from polluted regions

563   above the surface. The diurnal change of surface $PM_{2.5}$ concentration between EXP1 and

564   EXP1_E1 is very similar with slightly difference that results in their slight difference in DI in

565   the afternoon and night.

566

567   3.3.2 Impacts from emission injection height

568   Previous studies suggested that the injection height of emissions from power plants may

569   also affect the diurnal cycle of surface pollutant concentration, particularly for SO_2 (e.g., Wang

570   et al.,2010; Lin et al.,2012; Qi et al.,2012; Xu et al.,2014). Therefore, one sensitivity

571   experiment, EXP1_E2, is conducted with setting the anthropogenic emissions placed only in

572   the first layer of model. Figure 16 shows the spatial distribution of the difference in maximum

573   DI between EXP1 and EXP1_E2 over East China. Over most areas of East China, EXP1

574   simulates lower maximum DI than EXP1_E2, and the difference is primarily in spring and

575   summer. The impact of injection height is negligible in winter. The distribution of impacts

576   correlates highly with the distribution of power plant locations. The reduction of DI of surface

577   SO_2 concentration in EXP1 compared to EXP1_E2 is mainly due to more emissions are placed

578   above the PBL during the night (Fig. S10 in the supporting material). As shown in Table 2,

579   most of power plant emissions are placed below 500 m in EXP1. The larger impact in summer

580   than in winter is mainly due to the higher PBL height during the night in winter (Fig. 7).

581   Therefore, emissions are still placed within the PBL even with the injection height, which

582   results in the small difference of DI of surface SO_2 concentration between EXP1 and EXP1_E2.

583   For surface $PM_{2.5}$ concentration, the impact of emission injection height is even smaller and

584   only distinguishable in summer (Fig. S11 in the supporting material). Overall, impact from the

585   injection height of emission on the diurnal variation of surface $PM_{2.5}$ concentration is much

586   smaller than that from PBL mixing.

587

4. Summary and discussion

589   In this study, the observed characteristics of diurnal variation of surface $PM_{2.5}$

590   concentration over the YRD region of East China in four seasons of 2018 is examined based

591   on the hourly surface observations at 190 stations of the region. On regional average, the

592   observed diurnal variation is the weakest in winter and the strongest in autumn. In spring and

593   autumn, the observed patterns of diurnal variation are similar, showing the minimum surface

594    $PM_{2.5}$ concentration in the afternoon, consistent with previous studies (e.g., Zhang and Cao et

595   al.,2015; Liu et al.,2016; Guo et al.,2017). In summer, different from other seasons, the

596   observed diurnal variation shows the maximum surface $PM_{2.5}$ concentration near the noon time.

597   The WRF-Chem experiments are conducted over East China and the simulated diurnal

598   variations of surface $PM_{2.5}$ concentration are compared with the observations. The model

599   generally captures the observed seasonality of diurnal variation of surface $PM_{2.5}$ concentration,

600   except that in summer the model significantly overestimates the diurnal peak during the night

601 and produces opposite diurnal pattern with the minimum concentration near the noon time. The

602 model can generally reproduce the patterns with the minimum noontime concentration in

603 spring and autumn, but overestimates the observed nighttime peaks, particularly in autumn.

604 The modeling biases and the mechanisms driving the diurnal variation of surface $PM_{2.5}$

605 concentration in four seasons are further investigated. Emission and PBL mixing are found to

606 be the two dominant processes controlling the diurnal variation of surface $PM_{2.5}$ concentration

607 over the polluted areas, and the PBL mixing leads to the simulated diurnal pattern of surface

608 $PM_{2.5}$ concentration. More specifically, the simulations suggest that the PBL mixing of the

609 primary $PM_{2.5}$ determines the modelled diurnal variation of surface $PM_{2.5}$ concentration.

610 Although the observation of $PM_{2.5}$ components is not available to evaluate the diurnal variation

611 of primary $PM_{2.5}$, the diurnal variation of surface mixing ratio of CO that is normally used to

612 represent the primary pollutant supports the findings (Fig. S12 in the supporting material).

613   The modeling results are found sensitive to the PBL schemes and the vertical

614 configuration (i.e., the number of model layers within PBL) of simulations. However, none

615 of the PBL schemes in WRF-Chem can reduce the modeling biases in diurnal variation of

616 surface $PM_{2.5}$ concentration. Contrary to the intuition, more model layers within PBL worsen

617 the model performance, which is mainly due to that more layers within PBL makes the first

618 model layer thinner and enlarges the contribution from emission if PBL mixing is not

619 efficient. The analysis indicates that the PBL mixing coefficient instead of the PBL height

620 controls the PBL mixing in WRF-Chem, particularly during the night. Increasing the lower

621 limit of PBL mixing coefficient within the PBL can significantly reduce the modeling biases

622 in diurnal variation of surface $PM_{2.5}$ concentration, primarily during the night. In addition, it

623 can also reduce the modeling sensitivity to the model vertical configuration. The model

624 performance of daily mean surface $PM_{2.5}$ concentration is also largely improved when the

625 biases of diurnal variation are reduced. The diurnal variation of anthropogenic emissions and

626 injection height of power plant emissions can affect the diurnal cycle of surface $PM_{2.5}$

627 concentration to some extent, but the impact is much smaller than that of PBL mixing.

628   This study highlights the importance of modeling PBL mixing coefficient within PBL

629 in models like WRF-Chem that simulates the PBL mixing process based on the mixing

630 coefficient instead of PBL height. Some studies found that other models also overestimated

631 the diurnal variation of observed surface $PM_{2.5}$ concentration over East China (e.g., Cai et

632 al.,2011; Liu M et al.,2018). Our finding suggests that those models may also have the

633 problems in modeling PBL mixing during the night. Many of previous modeling and

634 observation studies focus on investigating the variation of PBL height and its interaction

635   with aerosol concentration (e.g., Sawyer et al., 2015; Ding et al, 2016; Li et al, 2017; Song

636   et al.,2018; Su et al., 2018). However, this study reveals that the PBL mixing flux is more

637   critical than PBL height in terms of understanding the mixing of pollutants within PBL,

638   particularly during the night, which can not only significantly affect the diurnal variation but

639   also the daily mean of surface pollutant concentration. The increase of PBL mixing during

640   the night reduces the modeling biases, which may suggest that the simulated PBL mixing

641   during the night in WRF-Chem is too weak. One possible reason may be due to urban heat

642   island effect that is not accounted in this study, because the observation sites are mostly at

643   urban or sub-urban areas. The test simulations with the current version of WRF-Chem using

644   Noah land surface model with urban effect can increase the nighttime PBL mixing

645   coefficient from 0.1 m^2/s to 1-10 m^2/s during some cases at urban areas, but the results are

646   sensitive to the urban schemes (not shown), which deserves investigation in future. Another

647   suggestion is that the PBL mixing of pollutants may not be able to follow directly the mixing

648   coefficient diagnosed by PBL parameterization for meteorology, which deserves further

649   investigation. The improvement of modeling PBL height is not enough for understanding

650   the PBL mixing of pollutants. This suggests that the understanding of PBL structure and

651   detailed mixing process are needed. Besides the observation or retrieval of PBL height,

652   observations of PBL characteristics are needed.

653   Although the sensitivity adjustment of PBL mixing coefficient during the night can

654   largely reduce the modeling biases in diurnal variation of surface $PM_{2.5}$ concentration, one

655   evident deficiency is that the model produces opposite diurnal pattern compared with

656   observations in summer. It needs to be noted that the WRF-Chem simulations conducted in

657   this study do not consider the SOA production that still has large uncertainties in

658   mechanisms. One sensitivity experiment with the SOA production shows that the model can

659   better represent the observed diurnal pattern of surface $PM_{2.5}$ concentration in summer

660   showing the maximum concentration in the daytime (Fig. S13 in the supporting material).

661   This indicates that the SOA production may be important for modeling the diurnal variation

662   of surface $PM_{2.5}$ concentration in summer over East China, which suggests more detailed

663   analysis of impact of SOA production on diurnal cycle of surface $PM_{2.5}$ concentration is

664   needed with observations. It is also noteworthy that the impact of SOA production on diurnal

665   variation of surface $PM_{2.5}$ concentration is only significant in summer, likely due to the

666   strong photochemistry activity in summer. Another uncertainty of the results in this study

667   may be related to emissions. Although the diurnal variation and injection height of emission

668   do not contribute significantly to the night time positive biases of surface $PM_{2.5}$

669 concentration, the emission uncertainties of primary PM may influence the diurnal cycle of
670 surface $PM_{2.5}$. For example, overestimation of primary PM emission can increase the diurnal
671 variation. Therefore, this study suggests that the long-term measurements of $PM_{2.5}$
672 components at more stations are needed to further investigate the characteristics of diurnal
673 variation of $PM_{2.5}$, which can improve our understanding of the impacts of multiple
674 processes, such as chemical production, emissions, and meteorology, on the formation and
675 evolution of air pollution.

676

Data availability

678   The release version of WRF-Chem can be download from
679 http://www2.mmm.ucar.edu/wrf/users/download/get_source.html. The updated USTC
680 version of WRF-Chem can be downloaded from http://aemol.ustc.edu.cn/product/list/ or
681 contact chunzhao@ustc.edu.cn. Also, the code modifications will be incorporated the release
682 version of WRF-Chem in future.

683

Author contributions

685   Qiuyan Du and Chun Zhao designed the experiments, conducted and analyzed the
686 simulations. All authors contributed to the discussion and final version of the paper.

687

Acknowledgements

689   This research was supported by the Fundamental Research Funds for the Central
690 Universities, and the National Natural Science Foundation of China (grant 41775146). The
691 study used the computing resources from the High-Performance Computing Center of
692 University of Science and Technology of China (USTC). Part of the observation data is from
693 the Qingyue Open Environmental Data Center (https://data.epmap.org).

694

695

696 **Reference**

697   Ackerman, T. P.: A Model of the Effect of Aerosols on Urban Climates with Particular
698   Applications to the Los Angeles Basin, J. Atmos. Sci., 34, 531–547, doi:10.1175/1520-
699   0469(1977)034<0531:AMOTEO>2.0.CO;2, 1977.
700   Arola, A., Eck, T. F., Huttunen, J., Lehtinen, K. E. J., Lindfors, A. V., Myhre, G., Smirnov,
701   A., Tripathi, S. N., and Yu, H.: Influence of observed diurnal cycles of aerosol optical
702   depth on aerosol direct radiative effect, Atmos. Chem. Phys., 13, 7895-7901, 2013.
703   Bacmeister, J. T., Wehner, M. F., Neale, R. B., Gettelman, A., Hannay, C., Lauritzen, P. H.,
704   Caron, J. M., and Truesdale, J. E.: Exploratory High-Resolution Climate Simulations
705   using the Community Atmosphere Model (CAM), J. Climate, 27, 3073–3099,
706   doi:10.1175/JCLI-D-13-00387.1, 2014.
707   Barnard, J. C., Fast, J. D., Paredes-Miranda, G., Arnott, W. P., and Laskin, A.: Technical Note:
708   Evaluation of the WRF-Chem "Aerosol Chemical to Aerosol Optical Properties" Module
709   using data from the MILAGRO campaign, Atmos. Chem. Phys., 10, 7325–7340,
710   doi:10.5194/acp-10-7325-2010, 2010.
711   Bei, N., Li, G., Huang, R., Cao, J., Meng, N., Feng, T., Liu, S., Zhang, T., Zhang, Q., and
712   Molina, L. T.: Typical synoptic situations and their impacts on the wintertime air
713   pollution in the Guanzhong basin, China, Atmos. Chem. Phys., 16, e7387, 2016.
714   Binkowski, F. S. and Shankar, U.: The Regional Particulate Matter Model: 1. Model
715   Description and Preliminary Results, J. Geophys. Res., 100, 26191–26209, 1995.
716   Cai, H. and Xie, S.: Traffic-related air pollution modeling during the 2008 Beijing Olympic
717   Games: the effects of an odd-even day traffic restriction scheme, The Science of the
718   total environment, 409, 1935–1948, doi:10.1016/j.scitotenv.2011.01.025, 2011.
719   Chapman, E. G., Gustafson, W. I., Easter, R. C., Barnard, J. C., Ghan, S. J., Pekour, M. S.,
720   and Fast, J. D.: Coupling aerosol-cloud-radiative processes in the WRF-Chem model:
721   investigating the radiative impact of elevated point sources, Atmos. Chem. Phys., 9,
722   945-964, 2008.
723   Chen, D., Cui, H., Zhao, Y., Yin, L., Lu, Y., and Wang, Q.: A two-year study of carbonaceous
724   aerosols in ambient $PM_{2.5}$ at a regional background site for western Yangtze River Delta,
725   China, Atmospheric Research, 183, 351–361, doi:10.1016/j.atmosres.2016.09.004,
726   2017.
727   Chen, S., Zhao, C., Qian, Y., Leung, L. R., Huang, J., Huang, Z., Bi, J., Zhang, W., Shi, J.,
728   Yang, L., Li, D., and Li, J.: Regional modeling of dust mass balance and radiative

forcing over East Asia using WRF-Chem, Aeolian Research, 15, 15–30, doi:10.1016/j.aeolia.2014.02.001, 2014.

Chen, T., He, J., Lu, X., She, J., and Guan, Z.: Spatial and Temporal Variations of PM$_{2.5}$ and Its Relation to Meteorological Factors in the Urban Area of Nanjing, China, International journal of environmental research and public health, 13, doi:10.3390/ijerph13090921, 2016.

Chen, W., Tang, H., and Zhao, H.: Diurnal, weekly and monthly spatial variations of air pollutants and air quality of Beijing, Atmospheric Environment, 119, 21–34, doi:10.1016/j.atmosenv.2015.08.040, 2015.

Cheng, Y., Zheng, G., Wei, C., Mu, Q., Zheng, B., Wang, Z., Gao, M., Zhang, Q., He, K., Carmichael, G., Pöschl, U., and Su, H.: Reactive nitrogen chemistry in aerosol water as a source of sulfate during haze events in China, Science advances, 2, e1601530, doi:10.1126/sciadv.1601530, 2016.

Davidson C I, Phalen R F, Solomon P A.: Airborne particulate matter and human health: A review, 39(8), 737–749, 2005.

Dentener, F., Kinne, S., Bond, T., Boucher, O., Cofala, J., Generoso, S., Ginoux, P., Gong, S., Hoelzemann, J. J., Ito, A., Marelli, L., Penner, J. E., Putaud, J.-P., Textor, C., Schulz, M., van der Werf, G. R., and Wilson, J.: Emissions of primary aerosol and precursor gases in the years 2000 and 1750, prescribed data-sets for AeroCom, Atmos. Chem. Phys., 6, 4321-4344, 2006.

Dickerson, R. R., Kondragunta, S., Stenchikov, G., Civerolo, K. L., Doddridge, B. G., and Holben, B. N.: The impact of aerosols on solar ultraviolet radiation and photochemical smog, Science (New York, N.Y.), 278, 827–830, doi:10.1126/science.278.5339.827, 1997.

Ding, A. J., Fu, C. B., Yang, X. Q., Sun, J. N., Petäjä, T., Kerminen, V. M., Wang, T., Xie, Y., Herrmann, E., Zheng, L. F., Nie, W., Liu, Q., Wei, X. L., Kulmala, M.: Intense atmospheric pollution modifies weather: a case of mixed biomass burning with fossil fuel combustion pollution in eastern China, Atmospheric Chemistry and Physics, 13, 10545–10554, 2013.

Du, Q., Faber, V., & Gunzburger, M.: Centroidal Voronoi tessellations: Applications and algorithms, SIAM review, 41, 637–676, 1999.

Easter, R. C., Ghan, S. J., Zhang, Y., Saylor, R. D., Chapman, E. G., Laulainen, N. S., Abdul-Razzak, H., Leung, L. R., Bian, X., and Zaveri, R. A.: MIRAGE: Model Description

762   and Evaluation of Aerosols and Trace Gases, J. Geophys. Res., 109, D20210,
763   doi:10.1029/2004JD004571, 2004.

764 Fast, J. D, Gustafson Jr., W. I., Easter, R. C., Zaveri, R. A., Barnard, J. C., Chapman, E. G.,
765   and Grell, G. A.: Evolution of ozone, particulates, and aerosol direct forcing in an urban
766   area using a new fully-coupled meteorology, chemistry, and aerosol model, J. Geophys.
767   Res., 111, D21305, doi:10.1029/2005JD006721, 2006.

768 Feng, J., Zhong, M., Xu, B., Du, Y., Wu, M., Wang, H., and Chen, C.: Concentrations,
769   seasonal and diurnal variations of black carbon in $PM_{2.5}$ in Shanghai, China,
770   Atmospheric Research, 147-148, 1–9, doi:10.1016/j.atmosres.2014.04.018, 2014.

771 Fu, Q., Zhuang, G., Wang, J., Xu, C., Huang, K., Li, J., Hou, B., Lu, T., and Streets, D. G.:
772   Mechanism of formation of the heaviest pollution episode ever recorded in the Yangtze
773   River   Delta,   China,   Atmospheric   Environment,   42,   2023–2036,
774   doi:10.1016/j.atmosenv.2007.12.002, 2008.

775 Gakidou, E., Afshin, A., Abajobir, A. A., Abate, K. H., Abbafati, C., Abbas, K. M., ... & Abu-
776   Raddad, L.: Global, regional, and national comparative risk assessment of 84 behavioural,
777   environmental and occupational, and metabolic risks or clusters of risks, 1990–2016: a
778   systematic analysis for the Global Burden of Disease Study 2016, The Lancet, 390, 1345-
779   1422, 2017.

780 Gao, Y., Liu, X., Zhao, C., and Zhang, M.: Emission controls versus meteorological
781   conditions in determining aerosol concentrations in Beijing during the 2008 Olympic
782   Games, Atmos. Chem. Phys., 11, 12437–12451, doi:10.5194/acp-11-12437-2011, 2011.

783 Gao, Y., Zhao, C., Liu, X., Zhang, M., and Leung, L. R.: WRF-Chem simulations of aerosols
784   and anthropogenic aerosol radiative forcing in East Asia, Atmospheric Environment,
785   92, 250–266, doi:10.1016/j.atmosenv.2014.04.038, 2014.

786 Geng, G., Zhang, Q., Martin, R. V., van Donkelaar, A., Huo, H., Che, H., Lin, J., and He, K.:
787   Estimating long-term $PM_{2.5}$ concentrations in China using satellite-based aerosol
788   optical depth and a chemical transport model, Remote Sensing of Environment, 166,
789   262–270, doi:10.1016/j.rse.2015.05.016, 2015.

790 Ginoux, P., Chin, M., Tegen, I., Prospero, J. M., Holben, B., Dubovik, O., and Lin, S.:
791   Sources and distributions of dust aerosols simulated with the GOCART model, J.
792   Geophys. Res., 106, 20225–20273, 2001.

793 Gong, D.Y., Ho, C.-H., Chen, D., Qian, Y., Choi, Y.-S., and Kim, J.: Weekly cycle of aerosol-
794   meteorology   interaction   over   China,   J.   Geophys.   Res.,   112,   L03819,
795   doi:10.1029/2007JD008888, 2007.

796   Gong, S. L.: A parameterization of sea-salt aerosol source function for sub- and super-micron
797   particles, Global Biogeochem. Cycles, 17, n/a-n/a, doi:10.1029/2003GB002079, 2003.

798   Grell, G. A., Peckham, S. E., Schmitz, R., and McKeen, S. A., Frost, G., Skamarock, W. C.,
799   and Eder, B.: Fully coupled "online" chemistry within the WRF model, Atmos.
800   Environ., 39, 6957–6976, 2005.

801   Gu, Z., Feng, J., Han, W., Li, L., Wu, M., Fu, J., and Sheng, G.: Diurnal variations of
802   polycyclic aromatic hydrocarbons associated with $PM_{2.5}$ in Shanghai, China, Journal of
803   environmental sciences (China), 22, 389–396, 2010.

804   Guo, H., Cheng, T., Gu, X., Wang, Y., Chen, H., Bao, F., Shi, S., Xu, B., Wang, W., Zuo, X.,
805   Zhang, X., and Meng, C.: Assessment of $PM_{2.5}$ concentrations and exposure throughout
806   China using ground observations, The Science of the total environment, 601-602,
807   1024–1030, doi:10.1016/j.scitotenv.2017.05.263, 2017.

808   Guo, J., Xia, F., Zhang, Y., Liu, H., Li, J., Lou, M., He, J., Yan, Y., Wang, F., Min, M., and
809   Zhai, P.: Impact of diurnal variability and meteorological factors on the $PM_{2.5}$ - AOD
810   relationship: Implications for $PM_{2.5}$ remote sensing, Environmental pollution (Barking,
811   Essex 1987), 221, 94–104, doi:10.1016/j.envpol.2016.11.043, 2017.

812   Gustafson, W. I., Chapman, E. G., Ghan, S. J., Easter, R. C., and Fast, J. D.: Impact on
813   modeled cloud characteristics due to simplified treatment of uniform cloud
814   condensation nuclei during NEAQS 2004, Geophys. Res. Lett., 34, L19809,
815   doi:10.1029/2007GL030021, 2007.

816   Ho, H. C., Wong, M. S., Yang, L., Shi, W., Yang, J., Bilal, M., and Chan, T.-C.:
817   Spatiotemporal influence of temperature, air quality, and urban environment on cause-
818   specific mortality during hazy days, Environment international, 112, 10–22,
819   doi:10.1016/j.envint.2017.12.001, 2018.

820   Hong, S.-Y., Noh, Y., and Dudhia, J.: A New Vertical Diffusion Package with an Explicit
821   Treatment of Entrainment Processes, Mon. Wea. Rev., 134, 2318–2341,
822   doi:10.1175/MWR3199.1, 2006.

823   Hu, J., Wang, Y., Ying, Q., and Zhang, H.: Spatial and temporal variability of $PM_{2.5}$ and PM_{10}
824   over the North China Plain and the Yangtze River Delta, China, Atmospheric
825   Environment, 95, 598–609, doi:10.1016/j.atmosenv.2014.07.019, 2014.

826   Hu, J., Chen, J., Ying, Q., and Zhang, H.: One-Year Simulation of Ozone and Particulate
827   Matter in China Using WRF/CMAQ Modeling System, Atmos. Chem. Phys., 16, 10333,
828   2016.

829 Hu, Z., Zhao, C., Huang, J., Leung, L. R., Qian, Y., Yu, H., Huang, L., and Kalashnikova, O.
830   V.: Trans-pacific transport and evolution of aerosols: Evaluation of quasi global WRF-
831   Chem simulation with multiple observations, Geosci. Model Dev. Discuss., 1–65,
832   doi:10.5194/gmd-2015-248, 2016.

833 Hu, Z., Huang, J., Zhao, C., Bi, J., Jin, Q., Qian, Y., Leung, L. R., Feng, T., Chen, S., and
834   Ma, J.: Modeling the contributions of Northern Hemisphere dust sources to dust
835   outflow from East Asia, Atmospheric Environment, 202, 234–243,
836   doi:10.1016/j.atmosenv.2019.01.022, 2019.

837 Huang, G., Cheng, T., Zhang, R., Tao, J., Leng, C., Zhang, Y., Zha, S., Zhang, D., Li, X., and
838   Xu, C.: Optical properties and chemical composition of $PM_{2.5}$ in Shanghai in the spring
839   of 2012, Particuology, 13, 52–59, doi:10.1016/j.partic.2013.10.005, 2014.

840 Huang, X., Ding, A., Liu, L., Liu, Q., Ding, K., Nie, W., Xu, Z., Chi, X., Wang, M., Sun, J.,
841   Guo, W., and Fu, C.: Effects of aerosol-radiation interaction on precipitation during
842   biomass-burning season in East China, Atmos. Chem. Phys., 16, 2016.

843 Huang, X.F., He, L.Y., Hu, M., Canagaratna, M. R., Sun, Y., Zhang, Q., Zhu, T., Xue, L.,
844   Zeng, L.-W., Liu, X.-G., Zhang, Y.-H., Jayne, J. T., Ng, N. L., and Worsnop, D. R.:
845   Highly time-resolved chemical characterization of atmospheric submicron particles
846   during 2008 Beijing Olympic Games using an Aerodyne High-Resolution Aerosol
847   Mass Spectrometer, Atmos. Chem. Phys., 10, 8933-8945, 2010.

848 Iacono, M. J., Mlawer, E. J., Clough, S. A., & Morcrette, J. J.: Impact of an improved
849   longwave radiation model, RRTM, on the energy budget and thermodynamic properties
850   of the NCAR community climate model, CCM3, Journal of Geophysical Research:
851   Atmospheres, 105, 14873-14890, 2000.

852 Jacobson, M. Z.: Studying the effects of aerosols on vertical photolysis rate coefficient and
853   temperature profiles over an urban airshed, J. Geophys. Res., 103, 10593–10604,
854   doi:10.1029/98JD00287, 1998.

855 Jaeglé, L., Quinn, P. K., Bates, T. S., Alexander, B., & Lin, J. T.: Global distribution of sea salt
856   aerosols: new constraints from in situ and remote sensing observations, Atmospheric
857   Chemistry and Physics, 11, 3137-3157, 2011.

858 Janssens-Maenhout, G., Crippa, M., Guizzardi, D., Dentener, F., Muntean, M., Pouliot, G.,
859   Keating, T., Zhang, Q., Kurokawa, J., Wankmüller, R., van der Denier Gon, H., Klimont,
860   Z., Frost, G., Darras, S., and Koffi, B.: HTAP_v2: a mosaic of regional and global
861   emission gridmaps for 2008 and 2010 to study hemispheric transport of air pollution,

Atmos. Chem. Phys. Discuss., 15, 12867–12909, doi:10.5194/acpd-15-12867-2015, 2015.

Jia, M., Zhao, T., Cheng, X., Gong, S., Zhang, X., Tang, L., Liu, D., Wu, X., Wang, L., and Chen, Y.: Inverse Relations of $PM_{2.5}$ and O_3 in Air Compound Pollution between Cold and Hot Seasons over an Urban Area of East China, Atmosphere, 8, 59, doi:10.3390/atmos8030059, 2017.

Jiang, F., Liu, Q., Huang, X., Wang, T., Zhuang, B., and Xie, M.: Regional modeling of secondary organic aerosol over China using WRF/Chem, Journal of Aerosol Science, 43, 57–73, doi:10.1016/j.jaerosci.2011.09.003, 2012.

Kain, J. S.: The Kain–Fritsch convective parameterization: An update, J. Appl. Meteorol., 43, 170–181, 2004.

Kassianov, E., Barnard, J., Pekour, M., Berg, L. K., Michalsky, J., Lantz, K., and Hodges, G.: Do diurnal aerosol changes affect daily average radiative forcing?, Geophys. Res. Lett., 40, 3265–3269, doi:10.1002/grl.50567, 2013.

Kok, J. F.: A scaling theory for the size distribution of emitted dust aerosols suggests climate models underestimate the size of the global dust cycle, Proceedings of the National Academy of Sciences of the United States of America, 108, 1016–1021, doi:10.1073/pnas.1014798108, 2011.

Kuang, Y., Zhao, C. S., Tao, J. C., and Ma, N.: Diurnal variations of aerosol optical properties in the North China Plain and their influences on the estimates of direct aerosol radiative effect, Atmos. Chem. Phys., 15, 5761–5772, doi:10.5194/acp-15-5761-2015, 2015.

Li, G., Wang, Y., Lee, K. H., Diao, Y., & Zhang, R.: Impacts of aerosols on the development and precipitation of a mesoscale squall line, Journal of Geophysical Research: Atmospheres, 114, 2009.

Li, J., Wang, G., Aggarwal, S. G., Huang, Y., Ren, Y., Zhou, B., Singh, K., Gupta, P. K., Cao, J., and Zhang, R.: Comparison of abundances, compositions and sources of elements, inorganic ions and organic compounds in atmospheric aerosols from Xi'an and New Delhi, two megacities in China and India, The Science of the total environment, 476-477, 485–495, doi:10.1016/j.scitotenv.2014.01.011, 2014.

Li, J., Yang, W., Wang, Z., Chen, H., Hu, B., Li, J., Sun, Y., Fu, P., and Zhang, Y.: Modeling study of surface ozone source-receptor relationships in East Asia, Atmospheric Research, 167, 77–88, doi:10.1016/j.atmosres.2015.07.010, 2016.

Li, M., Liu, H., Geng, G., Hong, C., Liu, F., Song, Y., ... & Zhang, Q.: Anthropogenic emission inventories in China: a review, National Science Review, 4, 834-866, 2017.

896   Li, M., Zhang, Q., Kurokawa, J.-i., Woo, J.-H., He, K., Lu, Z., Ohara, T., Song, Y., Streets,
897   D. G., Carmichael, G. R., Cheng, Y., Hong, C., Huo, H., Jiang, X., Kang, S., Liu, F., Su,
898   H., and Zheng, B.: MIX: a mosaic Asian anthropogenic emission inventory under the
899   international collaboration framework of the MICS-Asia and HTAP, Atmos. Chem.
900   Phys., 17, 935–963, doi:10.5194/acp-17-935-2017, 2017.
901   Li, P., Wang, L., Guo, P., Yu, S., Mehmood, K., Wang, S., Liu, W., Seinfeld, J. H., Zhang,
902   Y., Wong, D. C., Alapaty, K., Pleim, J., and Mathur, R.: High reduction of ozone and
903   particulate matter during the 2016 G-20 summit in Hangzhou by forced emission
904   controls of industry and traffic, Environ Chem Lett, 15, 709–715, doi:10.1007/s10311-
905   017-0642-2, 2017.
906   Li, R., Li, Z., Gao, W., Ding, W., Xu, Q., & Song, X.: Diurnal, seasonal, and spatial variation
907   of $PM_{2.5}$ in Beijing, Science Bulletin, 60, 387-395, 2015.
908   Li, T., Horton, R. M., Bader, D. A., Liu, F., Sun, Q., and Kinney, P. L.: Long-term projections
909   of temperature-related mortality risks for ischemic stroke, hemorrhagic stroke, and
910   acute ischemic heart disease under changing climate in Beijing, China, Environment
911   international, 112, 1–9, doi:10.1016/j.envint.2017.12.006, 2018.
912   Li, X., Zhang, Q., Zhang, Y., Zheng, B., Wang, K., Chen, Y., Wallington, T. J., Han, W., Shen,
913   W., Zhang, X., and He, K.: Source contributions of urban $PM_{2.5}$ in the Beijing–Tianjin–
914   Hebei region: Changes between 2006 and 2013 and relative impacts of emissions and
915   meteorology,   Atmospheric   Environment,   123,   229–239,
916   doi:10.1016/j.atmosenv.2015.10.048, 2015.
917   Li, Z., Guo, J., Ding, A., Liao, H., Liu, J., Sun, Y., ... & Zhu, B.: Aerosol and boundary-layer
918   interactions and impact on air quality, National Science Review, 4, 810-833, 2017.
919   Liao, J., Wang, T., Wang, X., Xie, M., Jiang, Z., Huang, X., and Zhu, J.: Impacts of different
920   urban canopy schemes in WRF/Chem on regional climate and air quality in Yangtze
921   River   Delta,   China,   Atmospheric   Research,   145-146,   226–243,
922   doi:10.1016/j.atmosres.2014.04.005, 2014.
923   Lin, M., Tao, J., Chan, C.-Y., Cao, J.-J., Zhang, Z.-S., Zhu, L.-H., and Zhang, R.-J.:
924   Regression Analyses between Recent Air Quality and Visibility Changes in Megacities
925   at Four Haze Regions in China, Aerosol Air Qual. Res., 12, 1049–1061,
926   doi:10.4209/aaqr.2011.11.0220, 2012.
927   Lin, W., Xu, X., Ma, Z., Zhao, H., Liu, X., and Wang, Y.: Characteristics and recent trends
928   of sulfur dioxide at urban, rural, and background sites in north China: effectiveness of
929   control measures, Journal of environmental sciences (China), 24, 34–49, 2012.

930 Liu, J., Li, J., and Li, W.: Temporal Patterns in Fine Particulate Matter Time Series in Beijing:
931   A Calendar View, Scientific reports, 6, 32221, doi:10.1038/srep32221, 2016.

932 Liu, M., Lin, J., Wang, Y., Sun, Y., Zheng, B., Shao, J., ... & Yan, Y.: Spatiotemporal
933   variability of NO 2 and PM$_{2.5}$ over Eastern China: observational and model analyses
934   with a novel statistical method, Atmospheric Chemistry and Physics, 18, 12933-12952,
935   2018.

936 Liu, S., Hua, S., Wang, K., Qiu, P., Liu, H., Wu, B., Shao, P., Liu, X., Wu, Y., Xue, Y., Hao,
937   Y., and Tian, H.: Spatial-temporal variation characteristics of air pollution in Henan of
938   China: Localized emission inventory, WRF/Chem simulations and potential source
939   contribution analysis, The Science of the total environment, 624, 396–406,
940   doi:10.1016/j.scitotenv.2017.12.102, 2018.

941 Liu, T., Cai, Y., Feng, B., Cao, G., Lin, H., Xiao, J., Li, X., Liu, S., Pei, L., Fu, L., Yang, X.,
942   Zhang, B., and Ma, W.: Long-term mortality benefits of air quality improvement during
943   the twelfth five-year-plan period in 31 provincial capital cities of China, Atmospheric
944   Environment, 173, 53–61, doi:10.1016/j.atmosenv.2017.10.054, 2018.

945 Liu, X.-Y., Zhang, Y., Zhang, Q., and He, K.-B.: Application of online-coupled WRF/Chem-
946   MADRID in East Asia: Model evaluation and climatic effects of anthropogenic
947   aerosols, Atmospheric Environment, 124, 321–336,
948   doi:10.1016/j.atmosenv.2015.03.052, 2016.

949 Ma, Q., Wu, Y., Tao, J., Xia, Y., Liu, X., Zhang, D., Han, Z., Zhang, X., and Zhang, R.:
950   Variations of Chemical Composition and Source Apportionment of PM$_{2.5}$ during Winter
951   Haze Episodes in Beijing, Aerosol Air Qual. Res., 17, 2791–2803,
952   doi:10.4209/aaqr.2017.10.0366, 2017.

953 Ma, Y., Xu, X., Song, W., Geng, F., and Wang, L.: Seasonal and diurnal variations of
954   particulate organosulfates in urban Shanghai, China, Atmospheric Environment, 85,
955   152–160, doi:10.1016/j.atmosenv.2013.12.017, 2014.

956 Menut, L., Goussebaile, A., Bessagnet, B., Khvorostiyanov, D., and Ung, A.: Impact of
957   realistic hourly emissions profiles on air pollutants concentrations modelled with
958   CHIMERE, Atmospheric Environment, 49, 233–244,
959   doi:10.1016/j.atmosenv.2011.11.057, 2012.

960 Miao, Y., Guo, J., Liu, S., Zhao, C., Li, X., Zhang, G., Wei, W., and Ma, Y.: Impacts of
961   synoptic condition and planetary boundary layer structure on the trans-boundary
962   aerosol transport from Beijing-Tianjin-Hebei region to northeast China, Atmospheric
963   Environment, 181, 1–11, doi:10.1016/j.atmosenv.2018.03.005, 2018.

964 Mlawer, E. J., S. J. Taubman, P. D. Brown, M. J. Iacono, and S. A. Clough.: Radiative
965   transfer for inhomogeneous atmosphere: RRTM, a validated correlated-k model for the
966   longwave, J. Geophys. Res., **102**, 16 663–16 682, 1997.
967 Morrison, H., Thompson, G., and Tatarskii, V.: Impact of Cloud Microphysics on the
968   Development of Trailing Stratiform Precipitation in a Simulated Squall Line:
969   Comparison of One- and TwoMoment Schemes, Mon. Weather Rev., 137, 991–1007,
970   2009.
971 Nakanishi, M. and Niino, H.: An Improved Mellor–Yamada Level-3 Model: Its Numerical
972   Stability and Application to a Regional Prediction of Advection Fog, Boundary-Layer
973   Meteorol, 119, 397–407, doi:10.1007/s10546-005-9030-8, 2006.
974 Ni, Z.-Z., Luo, K., Zhang, J.-X., Feng, R., Zheng, H.-X., Zhu, H.-R., Wang, J.-F., Fan, J.-R.,
975   Gao, X., and Cen, K.-F.: Assessment of winter air pollution episodes using long-range
976   transport modeling in Hangzhou, China, during World Internet Conference, 2015,
977   Environmental pollution (Barking, Essex 1987), 236, 550–561,
978   doi:10.1016/j.envpol.2018.01.069, 2018.
979 Olivier, J., Peters, J., Granier, C., Petron, G., Muller, J. F., and Wallens, S.: Present and Future
980   surface emissions of anthropogenic compounds, POET report #2, EU project EVK2-
981   1999-00011, 2003.
982 Pal, S., Lee, T. R., Phelps, S., and Wekker, S. F. J. de: Impact of atmospheric boundary layer
983   depth variability and wind reversal on the diurnal variability of aerosol concentration
984   at a valley site, The Science of the total environment, 496, 424–434,
985   doi:10.1016/j.scitotenv.2014.07.067, 2014.
986 Pathak, R. K., Wang, T., and Wu, W. S.: Nighttime enhancement of $PM_{2.5}$ nitrate in
987   ammonia-poor atmospheric conditions in Beijing and Shanghai: Plausible contributions
988   of heterogeneous hydrolysis of N_2O_5 and HNO_3 partitioning, Atmospheric
989   Environment, 45, 1183–1191, doi:10.1016/j.atmosenv.2010.09.003, 2011.
990 Pet äj ä, T., J ärvi, L., Kerminen, V.-M., Ding, A. J., Sun, J. N., Nie, W., Kujansuu, J., Virkkula,
991   A., Yang, X.-Q., Fu, C. B., Zilitinkevich, S., and Kulmala, M.: Enhanced air pollution
992   via aerosol-boundary layer feedback in China, Scientific reports, 6, 18998,
993   doi:10.1038/srep18998, 2016.
994 Pope III C A, Dockery D W.: Health effects of fine particulate air pollution: lines that connect,
995   Journal of the air & waste management association, 56, 709-742, 2006.

996 Qi, H., Lin, W., Xu, X., Yu, X., and Ma, Q.: Significant downward trend of SO_2 observed
997   from 2005 to 2010 at a background station in the Yangtze Delta region, China, Sci.
998   China Chem., 55, 1451–1458, doi:10.1007/s11426-012-4524-y, 2012.

999 Quan, J., Gao, Y., Zhang, Q., Tie, X., Cao, J., Han, S., Meng, J., Chen, P., and Zhao, D.:
1000   Evolution of planetary boundary layer under different weather conditions, and its
1001   impact on aerosol concentrations, Particuology, 11, 34–40,
1002   doi:10.1016/j.partic.2012.04.005, 2013.

1003 Roig Rodelas, R., Perdrix, E., Herbin, B., and Riffault, V.: Characterization and variability
1004   of inorganic aerosols and their gaseous precursors at a suburban site in northern France
1005   over one year (2015–2016), Atmospheric Environment, 200, 142–157,
1006   doi:10.1016/j.atmosenv.2018.11.041, 2019.

1007 Sawyer V R. Interaction between aerosol and the planetary boundary layer depth at sites in
1008   the US and China[C]//AGU Fall Meeting Abstracts. 2015.

1009 Seaman, N. L., Stauffer, D. R., and Lario-Gibbs, A. M.: A Multiscale Four-Dimensional Data
1010   Assimilation System Applied in the San Joaquin Valley during SARMAP. Part I:
1011   Modeling Design and Basic Performance Characteristics, J. Appl. Meteor., 34, 1739–
1012   1761, doi:10.1175/1520-0450(1995)034<1739:AMFDDA>2.0.CO;2, 1995.

1013 Seaton, A., MacNee, W., Donaldson, K., and Godden, D.: Particulate air pollution and acute
1014   health effects, Lancet (London, England), 345, 176–178, doi:10.1016/s0140-
1015   6736(95)90173-6, 1995.

1016 Shao, J., Chen, Q., Wang, Y., Lu, X., He, P., Sun, Y., Shah, V., Martin, R. V., Philip, S., Song,
1017   S., Zhao, Y., Xie, Z., Zhang, L., and Alexander, B.: Heterogeneous sulfate aerosol
1018   formation mechanisms during wintertime Chinese haze events: air quality model
1019   assessment using observations of sulfate oxygen isotopes in Beijing, Atmos. Chem.
1020   Phys., 19, 6107–6123, doi:10.5194/acp-19-6107-2019, 2019.

1021 Song, J., Xia, X., Che, H., Wang, J., Zhang, X., and Li, X.: Daytime variation of aerosol
1022   optical depth in North China and its impact on aerosol direct radiative effects,
1023   Atmospheric Environment, 182, 31–40, doi:10.1016/j.atmosenv.2018.03.024, 2018.

1024 Stauffer, D. R. and Seaman, N. L.: Use of four-dimensional data assimilation in a limited-
1025   area mesoscale model, Part I: Experiments with synoptic-scale data, Mon. Weather
1026   Rev., 118, 1250–1277, 1990.

Su, T., Li, Z., and Kahn, R.: Relationships between the planetary boundary layer height and surface pollutants derived from lidar observations over China, Atmos. Chem. Phys., 18, 15921-15935, 2018.

Sun, Y. L., Wang, Z. F., Du, W., Zhang, Q., Wang, Q. Q., Fu, P. Q., Pan, X. L., Li, J., Jayne, J., and Worsnop, D. R.: Long-term real-time measurements of aerosol particle composition in Beijing, China: seasonal variations, meteorological effects, and source analysis, Atmos. Chem. Phys., 15, 10149-10165, 2015.

Tao, M., Chen, L., Li, R., Wang, L., Wang, J., Wang, Z., Tang, G., and Tao, J.: Spatial oscillation of the particle pollution in eastern China during winter: Implications for regional air quality and climate, Atmospheric Environment, 144, 100–110, doi:10.1016/j.atmosenv.2016.08.049, 2016.

Tao, W., Liu, J., Ban-Weiss, G. A., Hauglustaine, D. A., Zhang, L., Zhang, Q., Cheng, Y., Yu, Y., and Tao, S.: Effects of urban land expansion on the regional meteorology and air quality of Eastern China, Atmos. Chem. Phys., 15, 8597-8614, 2015.

Tiwari, S., Srivastava, A. K., Bisht, D. S., Parmita, P., Srivastava, M. K., and Attri, S. D.: Diurnal and seasonal variations of black carbon and $PM_{2.5}$ over New Delhi, India: Influence of meteorology, Atmospheric Research, 125-126, 50–62, doi:10.1016/j.atmosres.2013.01.011, 2013.

Verma, V., Ning, Z., Cho, A. K., Schauer, J. J., Shafer, M. M., and Sioutas, C.: Redox activity of urban quasi-ultrafine particles from primary and secondary sources, Atmospheric Environment, 43, 6360–6368, doi:10.1016/j.atmosenv.2009.09.019, 2009.

Wang, G., Zhang, R., Gomez, M. E., Yang, L., Levy Zamora, M., Hu, M., Lin, Y., Peng, J., Guo, S., Meng, J., Li, J., Cheng, C., Hu, T., Ren, Y., Wang, Y., Gao, J., Cao, J., An, Z., Zhou, W., Li, G., Wang, J., Tian, P., Marrero-Ortiz, W., Secrest, J., Du, Z., Zheng, J., Shang, D., Zeng, L., Shao, M., Wang, W., Huang, Y., Wang, Y., Zhu, Y., Li, Y., Hu, J., Pan, B., Cai, L., Cheng, Y., Ji, Y., Zhang, F., Rosenfeld, D., Liss, P. S., Duce, R. A., Kolb, C. E., and Molina, M. J.: Persistent sulfate formation from London Fog to Chinese haze, Proceedings of the National Academy of Sciences of the United States of America, 113, 13630–13635, doi:10.1073/pnas.1616540113, 2016.

Wang, J., Christopher, S. A., Nair, U. S., Reid, J. S., Prins, E. M., Szykman, J., & Hand, J. L.: Mesoscale modeling of Central American smoke transport to the United States: 1."Top-down" assessment of emission strength and diurnal variation impacts, Journal of Geophysical Research: Atmospheres, 111, 2006.

Wang, T., Jiang, F., Deng, J., Shen, Y., Fu, Q., Wang, Q., Fu, Y., Xu, J., and Zhang, D.: Urban air quality and regional haze weather forecast for Yangtze River Delta region, Atmospheric Environment, 58, 70–83, doi:10.1016/j.atmosenv.2012.01.014, 2012.

Wang, X., Liang, X.-Z., Jiang, W., Tao, Z., Wang, J. X.L., Liu, H., Han, Z., Liu, S., Zhang, Y., and Grell, G. A.: WRF-Chem simulation of East Asian air quality: Sensitivity to temporal and vertical emissions distributions, Atmospheric Environment, 44, 660–669, doi:10.1016/j.atmosenv.2009.11.011, 2010.

Wang, X.P., Mauzerall, D. L., Hu, Y., Russell, A. G., Larson, E. D., Woo, J.-H., Streets, D. G., and Guenther, A.: A high-resolution emission inventory for eastern China in 2000 and three scenarios for 2020, Atmospheric Environment, 39, 5917–5933, doi:10.1016/j.atmosenv.2005.06.051, 2005.

Wang, Y.G., Ying, Q., Hu, J., and Zhang, H.: Spatial and temporal variations of six criteria air pollutants in 31 provincial capital cities in China during 2013–2014, Environment international, 73, 413–422, doi:10.1016/j.envint.2014.08.016, 2014.

Wang, Y.J., Li, L., Chen, C., Huang, C., Huang, H., Feng, J., Wang, S., Wang, H., Zhang, G., Zhou, M., Cheng, P., Wu, M., Sheng, G., Fu, J., Hu, Y., Russell, A. G., and Wumaer, A.: Source apportionment of fine particulate matter during autumn haze episodes in Shanghai, China, J. Geophys. Res. Atmos., 119, 1903–1914, doi:10.1002/2013JD019630, 2014.

Wang, Y.X., Zhang, Q., Jiang, J., Zhou, W., Wang, B., He, K., Duan, F., Zhang, Q., Philip, S., and Xie, Y.: Enhanced sulfate formation during China's severe winter haze episode in January 2013 missing from current models, J. Geophys. Res. Atmos., 119, 10,425-10,440, doi:10.1002/2013JD021426, 2014.

Wang, Z., Liu, D., Wang, Y., and Shi, G.: Diurnal aerosol variations do affect daily averaged radiative forcing under heavy aerosol loading observed in Hefei, China, Atmos. Meas. Tech., 8, 2901–2907, doi:10.5194/amt-8-2901-2015, 2015.

Wang, Z.F., Li, J., Wang, Z., Yang, W., Tang, X., Ge, B., Yan, P., Zhu, L., Chen, X., Chen, H., Wand, W., Li, J., Liu, B., Wang, X., Zhao, Y., Lu, N., and Su, D.: Modeling study of regional severe hazes over mid-eastern China in January 2013 and its implications on pollution prevention and control, Sci. China Earth Sci., 57, 3–13, doi:10.1007/s11430-013-4793-0, 2014.

Wiedinmyer, C., Akagi, S. K., Yokelson, R. J., Emmons, L. K., Al-Saadi, J. A., Orlando, J. J., and Soja, A. J.: The Fire INventory from NCAR (FINN) – a high resolution global

1093   model to estimate the emissions from open burning, Geosci. Model Dev. Discuss., 3,
1094   2439–2476, doi:10.5194/gmdd-3-2439-2010, 2010.

1095   Wu, L., Su, H., and Jiang, J. H.: Regional simulation of aerosol impacts on precipitation
1096   during the East Asian summer monsoon, J. Geophys. Res. Atmos., 118, 6454–6467,
1097   doi:10.1002/jgrd.50527, 2013.

1098   Xie, Y., Zhao, B., Zhang, L., and Luo, R.: Spatiotemporal variations of $PM_{2.5}$ and PM_{10}
1099   concentrations between 31 Chinese cities and their relationships with SO_2, NO_2, CO
1100   and O_3, Particuology, 20, 141–149, doi:10.1016/j.partic.2015.01.003, 2015.

1101   Xu, W. Y., Zhao, C. S., Ran, L., Lin, W. L., Yan, P., & Xu, X. B.: SO_2 noontime-peak
1102   phenomenon in the North China Plain, Atmospheric Chemistry and Physics, 14, 7757-
1103   7768, 2014.

1104   Xu, W., Sun, Y., Wang, Q., Zhao, J., Wang, J., Ge, X., Xie, C., Zhou, W., Du, W., Li, J., Fu,
1105   P., Wang, Z., Worsnop, D. R., and Coe, H.: Changes in Aerosol Chemistry From 2014
1106   to 2016 in Winter in Beijing: Insights From High-Resolution Aerosol Mass
1107   Spectrometry, J. Geophys. Res. Atmos., 124, 1132–1147, doi:10.1029/2018JD029245,
1108   2019.

1109   Yang Y, Liao H, Lou S.: Increase in winter haze over eastern China in recent decades: Roles
1110   of variations in meteorological parameters and anthropogenic emissions, Journal of
1111   Geophysical Research: Atmospheres, 121,050-13,065, 2016.

1112   Yang, Y., Smith, S. J., Wang, H., Lou, S., and Rasch, P. J.: Impact of Anthropogenic Emission
1113   Injection Height Uncertainty on Global Sulfur Dioxide and Aerosol Distribution, J.
1114   Geophys. Res. Atmos., 124, 4812–4826, doi:10.1029/2018JD030001, 2019.

1115   Ying, Z., Tie, X., and Li, G.: Sensitivity of ozone concentrations to diurnal variations of
1116   surface emissions in Mexico City: A WRF/Chem modeling study, Atmospheric
1117   Environment, 43, 851–859, doi:10.1016/j.atmosenv.2008.10.044, 2009.

1118   Zaveri, R. A. and Peters, L. K.: A new lumped structure photochemical mechanism for large-
1119   scale applications, J. Geophys. Res., 104, 30387–30415, doi:10.1029/1999JD900876,
1120   1999.

1121   Zaveri, R. A., Easter, R. C., Fast, J. D., & Peters, L. K.: Model for simulating aerosol
1122   interactions and chemistry (MOSAIC), Journal of Geophysical Research:
1123   Atmospheres, 113, 2008.

1124   Zhang, B., Wang, Y., and Hao, J.: Simulating aerosol–radiation–cloud feedbacks on
1125   meteorology and air quality over eastern China under severe haze conditionsin winter,
1126   Atmos. Chem. Phys., 15, 2387–2404, doi:10.5194/acp-15-2387-2015, 2015.

1127   Zhang, H., Wang, Y., Hu, J., Ying, Q., and Hu, X.-M.: Relationships between meteorological
1128   parameters and criteria air pollutants in three megacities in China, Environmental
1129   research, 140, 242–254, doi:10.1016/j.envres.2015.04.004, 2015.

1130   Zhang, L., Liao, H., and Li, J.: Impacts of Asian summer monsoon on seasonal and
1131   interannual variations of aerosols over eastern China, J. Geophys. Res., 115, D10307,
1132   doi:10.1029/2009JD012299, 2010.

1133   Zhang, L., Wang, T., Lv, M., and Zhang, Q.: On the severe haze in Beijing during January
1134   2013: Unraveling the effects of meteorological anomalies with WRF-Chem,
1135   Atmospheric Environment, 104, 11–21, doi:10.1016/j.atmosenv.2015.01.001, 2015.

1136   Zhang, R., Li, G., Fan, J., Wu, D. L., and Molina, M. J.: Intensification of Pacific storm track
1137   linked to Asian pollution, Proceedings of the National Academy of Sciences of the
1138   United States of America, 104, 5295–5299, doi:10.1073/pnas.0700618104, 2007.

1139   Zhang, Y., Zhang, X., Wang, L., Zhang, Q., Duan, F., and He, K.: Application of WRF/Chem
1140   over East Asia: Part I. Model evaluation and intercomparison with MM5/CMAQ,
1141   Atmospheric Environment, 124, 285–300, doi:10.1016/j.atmosenv.2015.07.022, 2016.

1142   Zhang, Y.-L. and Cao, F.: Fine particulate matter ($PM_{2.5}$) in China at a city level, Scientific
1143   reports, 5, 14884, doi:10.1038/srep14884, 2015.

1144   Zhao, B., Liou, K.-N., Gu, Y., Li, Q., Jiang, J. H., Su, H., He, C., Tseng, H.-L. R., Wang, S.,
1145   Liu, R., Qi, L., Lee, W.-L., and Hao, J.: Enhanced $PM_{2.5}$ pollution in China due to
1146   aerosol-cloud interactions, Scientific reports, 7, 4453, doi:10.1038/s41598-017-04096-
1147   8, 2017.

1148   Zhao, C., Liu, X., Leung, L. R., Johnson, B., McFarlane, S. A., Gustafson, W. I., Fast, J. D.,
1149   and Easter, R.: The spatial distribution of mineral dust and its shortwave radiative
1150   forcing over North Africa: modeling sensitivities to dust emissions and aerosol size
1151   treatments, Atmospheric Chemistry and Physics, 10, 8821-8838, 2010.

1152   Zhao, C., Liu, X., Leung, L. R., and Hagos, S.: Radiative impact of mineral dust on monsoon
1153   precipitation variability over West Africa, Atmospheric Chemistry and Physics, 11,
1154   1879-1893, 2011.

1155   Zhao C, Liu X, Leung L R.: Impact of the Desert dust on the summer monsoon system over
1156   Southwestern North America, Atmospheric Chemistry and Physics, 12, 3717-3731, 2012.

1157   Zhao, C., Chen, S., Leung, L. R., Qian, Y., Kok, J., Zaveri, R., and Huang, J.: Uncertainty in
1158   modeling dust mass balance and radiative forcing from size parameterization,
1159   Atmospheric Chemistry and Physics, 13, 10733-10753, 2013a.

1160 Zhao, C., Ruby Leung, L., Easter, R., Hand, J., and Avise, J.: Characterization of speciated
1161   aerosol direct radiative forcing over California, J. Geophys. Res. Atmos., 118, 2372–
1162   2388, doi:10.1029/2012JD018364, 2013b.

1163 Zhao, C., Hu, Z., Qian, Y., Leung, L. R., Huang, J., Huang, M., Jin, J., Flanner, M., Zhang,
1164   R., Wang, H., Yan, H., Lu, Z., and Streets, D. G.: Simulating black carbon and dust and
1165   their radiative forcing in seasonal snow: a case study over North China with field
1166   campaign measurements, Atmospheric Chemistry and Physics, 14, 11475-11491, 2014.

1167 Zhao, C., Huang, M., Fast, J. D., Berg, L. K., Qian, Y., Guenther, A., ... & Pfister, G.:
1168   Sensitivity of biogenic volatile organic compounds to land surface parameterizations and
1169   vegetation distributions in California, Geosci. Model Dev, 9, 1959-1976, 2016.

1170 Zhao, S., Yu, Y., Yin, D., He, J., Liu, N., Qu, J., and Xiao, J.: Annual and diurnal variations
1171   of gaseous and particulate pollutants in 31 provincial capital cities based on in situ air
1172   quality monitoring data from China National Environmental Monitoring Center,
1173   Environment international, 86, 92–106, doi:10.1016/j.envint.2015.11.003, 2016.

1174 Zhou, G., Xu, J., Xie, Y., Chang, L., Gao, W., Gu, Y., and Zhou, J.: Numerical air quality
1175   forecasting over eastern China: An operational application of WRF-Chem,
1176   Atmospheric Environment, 153, 94–108, doi:10.1016/j.atmosenv.2017.01.020, 2017.

1177 Zhou, G., Yang, F., Geng, F., Xu, J., Yang, X., Tie, X.: Measuring and modeling aerosol:
1178   relationship with haze events in Shanghai, China, Aerosol and air quality research, 14,
1179   783-792, 2014.

1180 **Table 1** Numerical experiments conducted in this study.

Name	PBL scheme	Vertical structure	PBL mixing coefficient (m^2/s)	Emission diurnal cycle	Emission injection height
CTL1	MYNN	layer1	Minimum=0.1	Yes	Yes
CTL2	MYNN	layer2	Minimum=0.1	Yes	Yes
CTL3	YSU	layer2	Minimum=0.1	Yes	Yes
EXP1	MYNN	layer1	Minimum = 5.0	Yes	Yes
EXP2	MYNN	layer2	Minimum = 5.0	Yes	Yes
EXP1_E1	MYNN	layer1	Minimum = 5.0	No	Yes
EXP1_E2	MYNN	layer1	Minimum = 5.0	Yes	No

1181

1182

1183 **Table 2** Vertical distributions of power plant emissions: percentage of each species allocated

1184 to the height of the vertical layers in the WRF-Chem model.

Species	Height of Emission Layers (m)				
	0-76	76-153	153-308	308-547	547-871
SO_2	5	30	35	25	5
NO_x	5	40	25	25	5
CO	5	70	20	5	0
NH_3	5	75	15	5	0
NMVOC	5	85	10	0	0
$PM_{2.5}$	5	45	25	20	5
PM_{10}	5	55	20	15	5
OC	5	70	15	10	0
BC	5	65	20	10	0

1185

1186
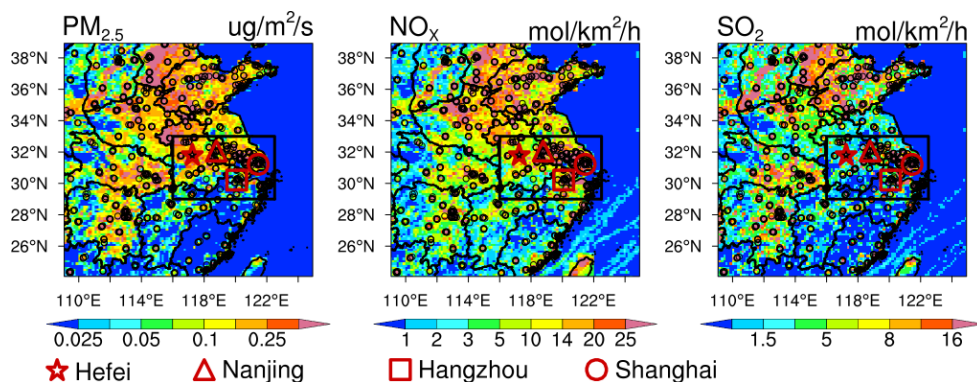
Figure 1a. MEIC China emission of SO_2, NO_2, $PM_{2.5}$ over the simulation domain (109.0°

E~124.9°E, 24.0°N~38.9°N) with black boxes showing the analyzed domain (116.0°E~122.5°

E, 29.0°N~33.0°N), overlaid with observational sites and four cities as the Center (Shanghai,

121.45 °E and 31.21 °N) and sub-Center (Nanjing, 118.78 °E and 32.06 °N; Hefei, 117.25 °E and

31.85 °N; Hangzhou, 120.08 °E and 30.21 °N) of the YRD city cluster.
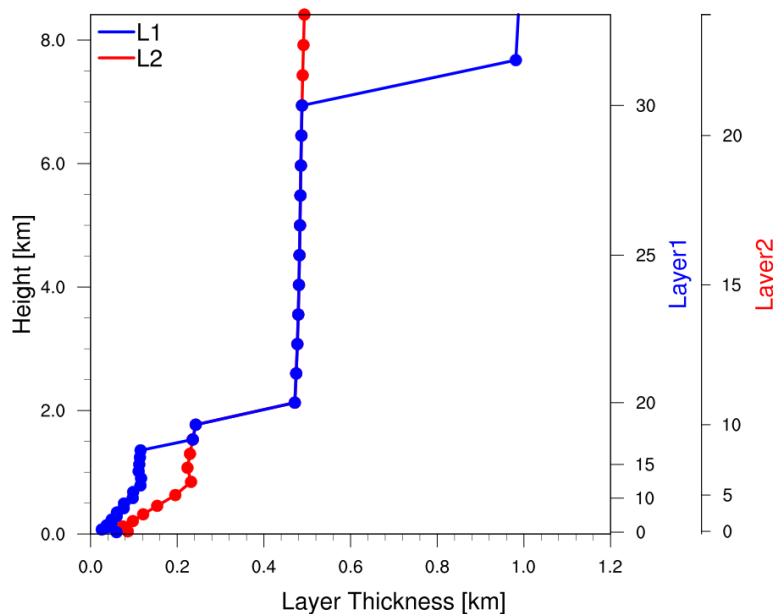
Figure 1b. Vertical profiles of the layer thickness from L1 and L2 layer configuration.
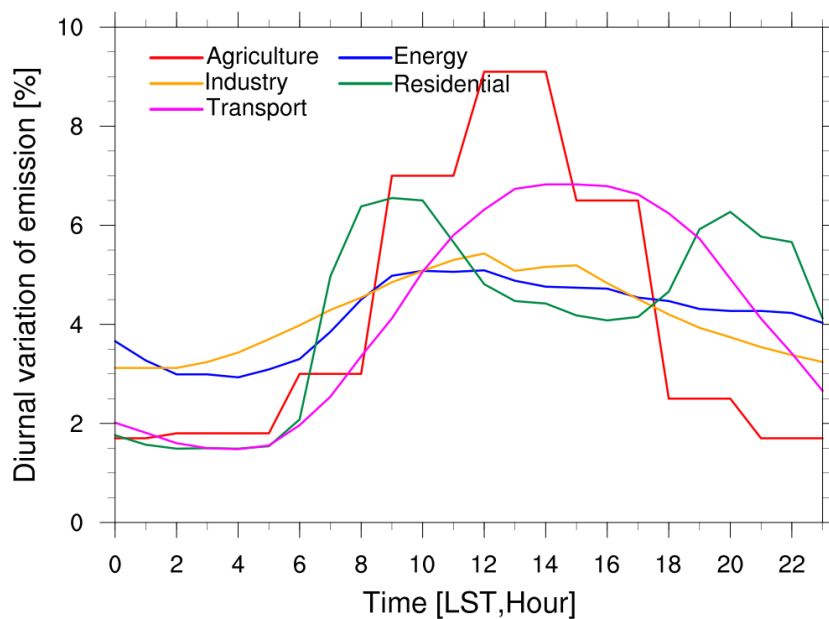
1200
1201 **Figure 1c**. Diurnal profiles of emissions from five individual sector (agriculture, industry,

1202 transport, energy, and residential).

1203

1204

1205

1206

1207

1208

1209

1210

1211
1212
1213
1214
1215
1216
1217
1218
1219
1220
1221
1222
1223
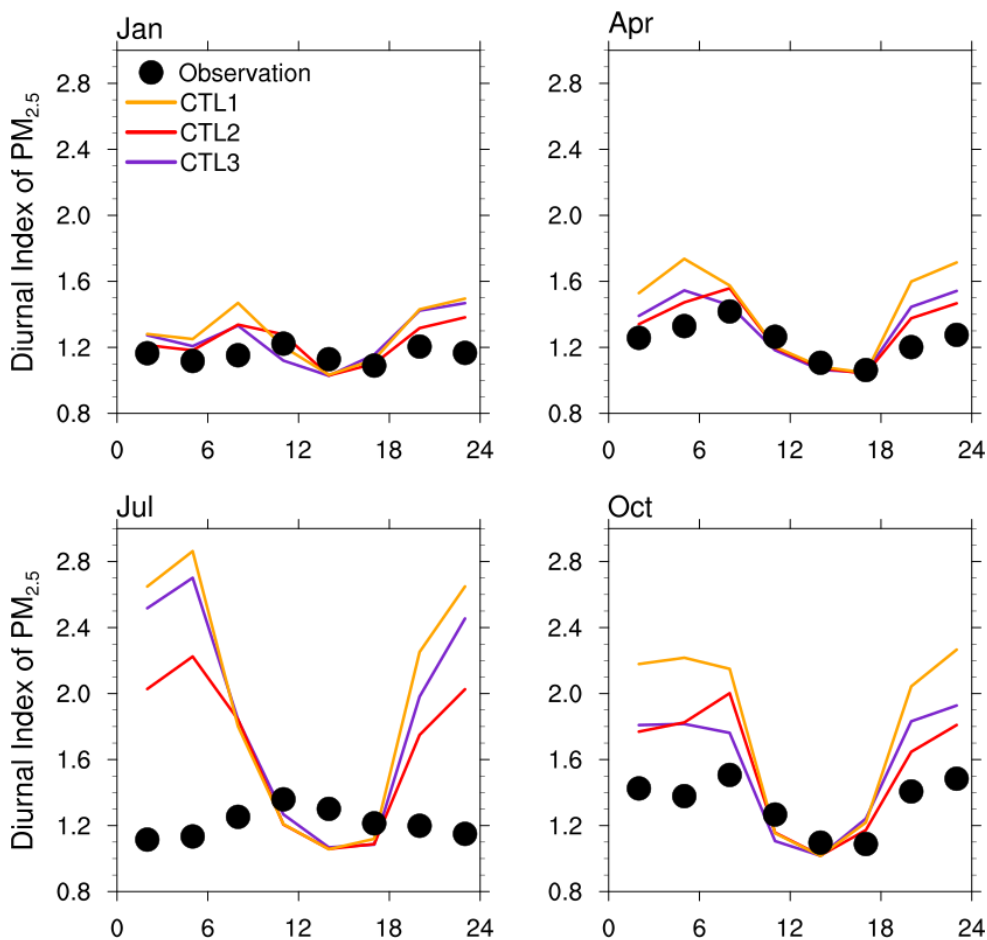
Figure 2. Diurnal index of surface PM$_{2.5}$ concentration within 24-hour averaged over the YRD region of East China (within black box of Fig. 1a) for January, April, July, and October of 2018 from the experiments CTL1, CTL2, CTL3, and observations. The simulated results are from 3-hourly output and sampled at the observational sites.

1234
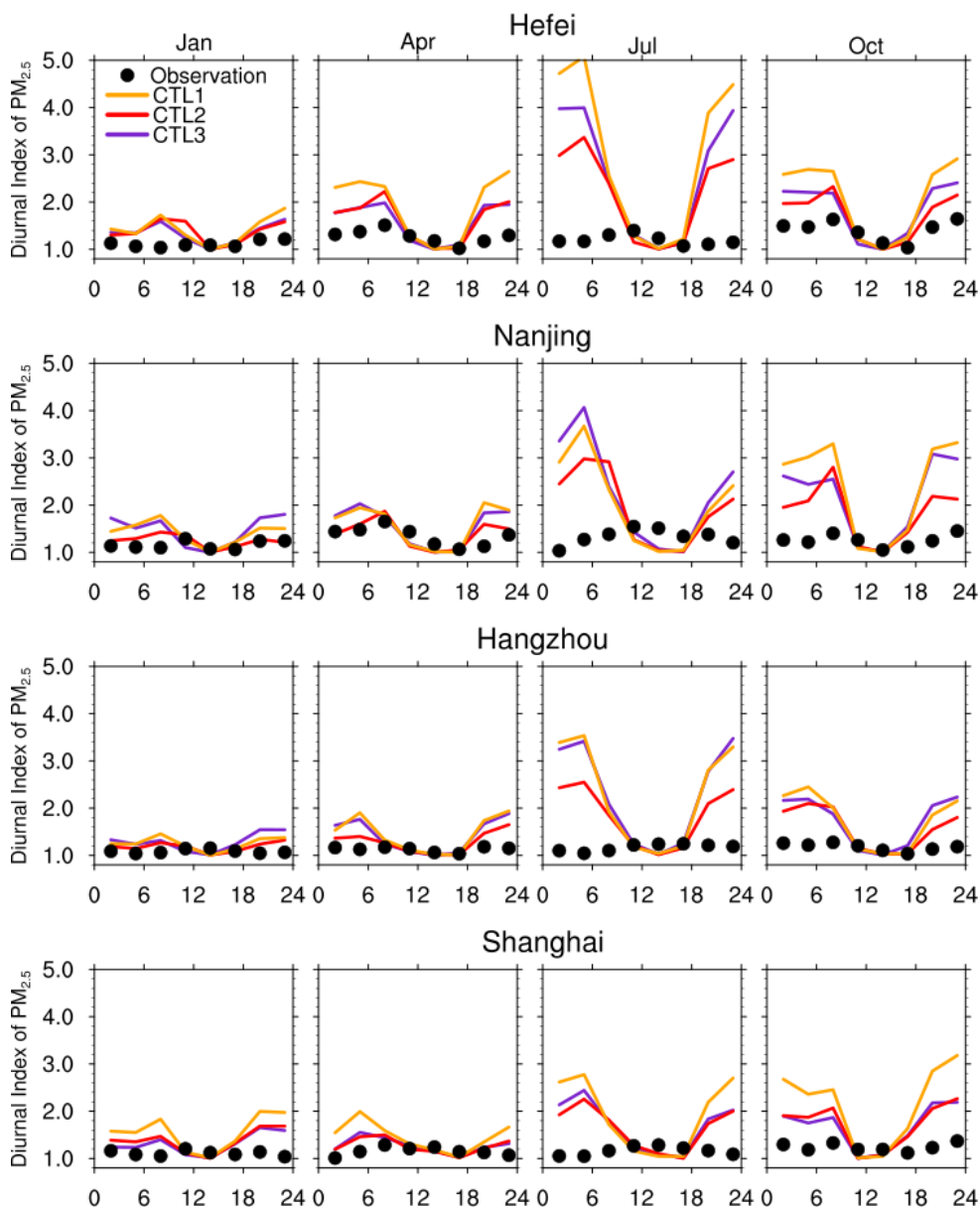
1235
1236 **Figure 3.** Diurnal index of surface PM$_{2.5}$ concentration within 24-hour averaged over four cities

1237 (Hefei, Nanjing, Hangzhou, Shanghai) for January, April, July, and October of 2018 from the

1238 experiments CTL1, CTL2, CTL3, and observations.

1239

1240

1241

1242
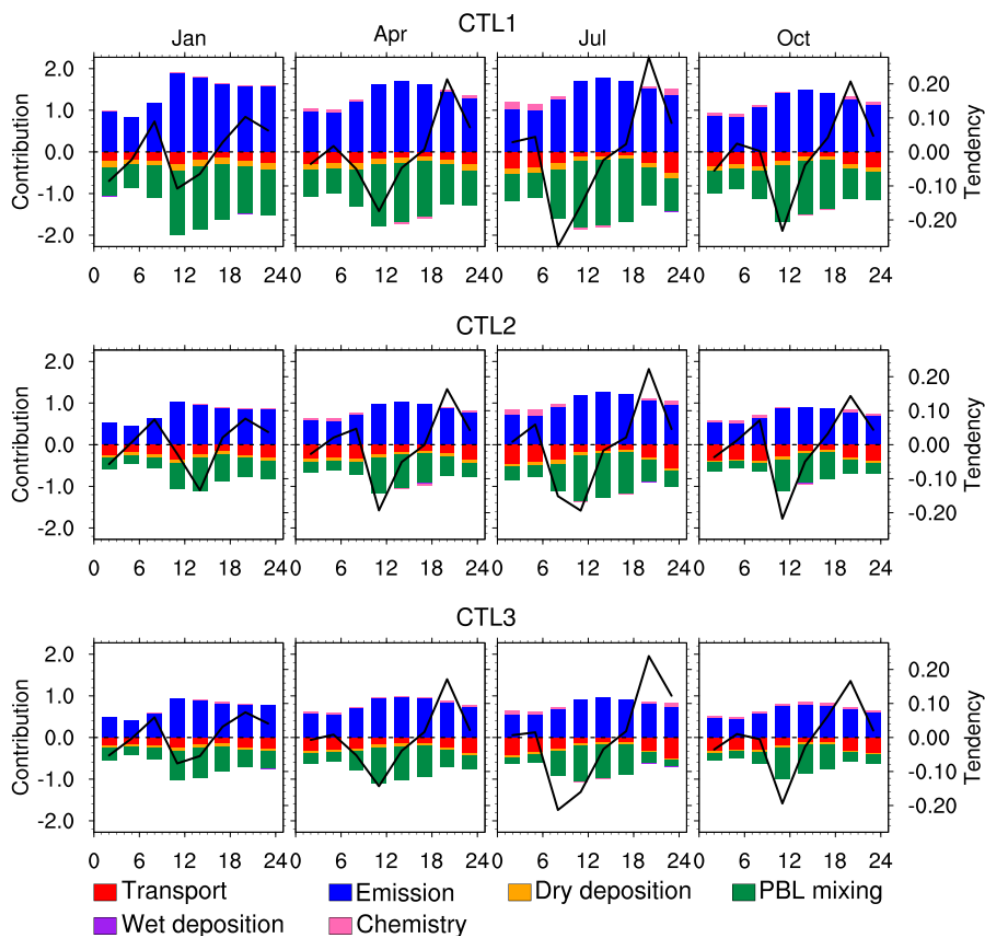
1244
1245 **Figure 4.** Contribution to surface PM$_{2.5}$ concentration every 3-hour from individual process

1246 (transport, emission, dry and wet deposition, PBL mixing, chemical production/loss) averaged

1247 over Hefei for January, April, July, and October of 2018 from the experiments CTL1, CTL2,

1248 and CTL3. The 3-hourly tendency of surface PM$_{2.5}$ concentration is also shown.

1249

1250

1251

1252

1253

1254

1255

1256

1257
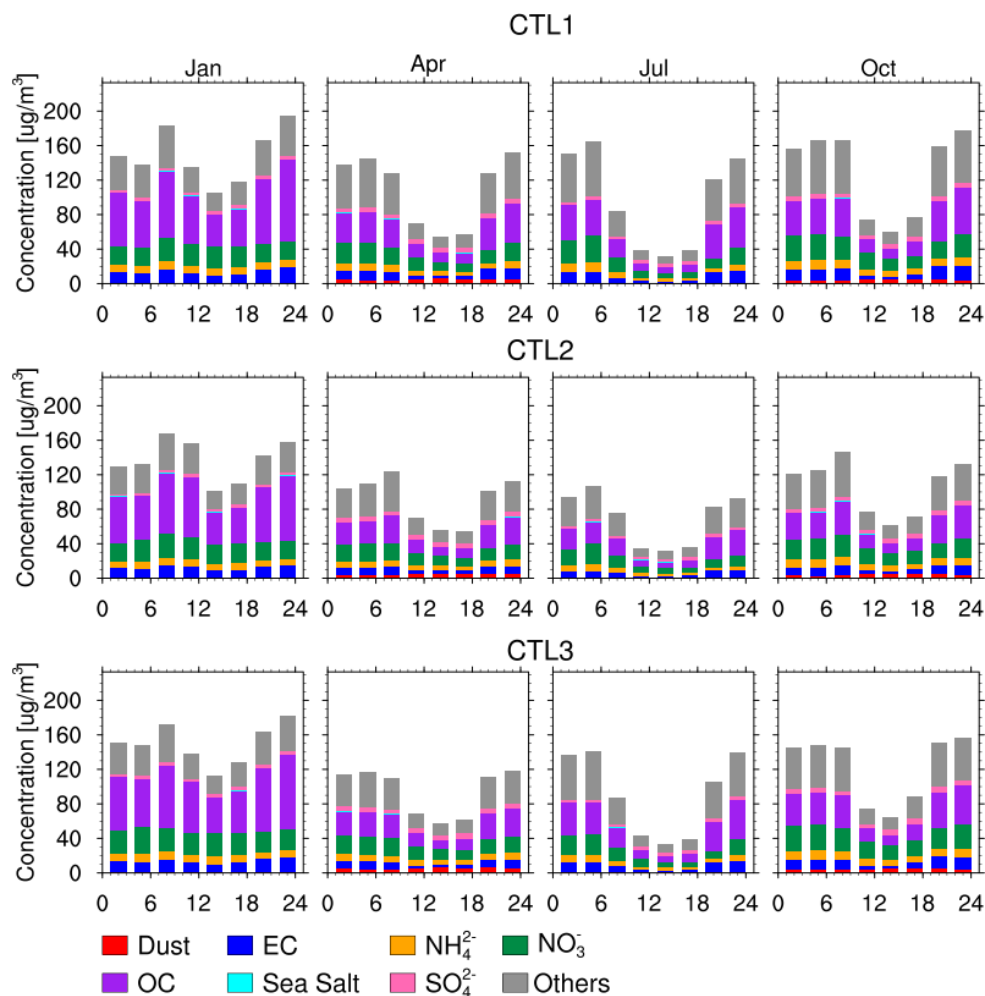
1258
1259 **Figure 5.** Diurnal variation of surface concentration of each PM$_{2.5}$ composition (Dust, OC, EC,

1260 Sea Salt, NH$_4{}^{2-}$, SO$_4{}^{2-}$, NO$_3{}^{-}$, and other inorganics) averaged over Hefei for January, April, July,

1261 and October of 2018 from the experiments CTL1, CTL2, and CTL3.

1262

1263

1264

1265

1266

1267

1268

1269

1270
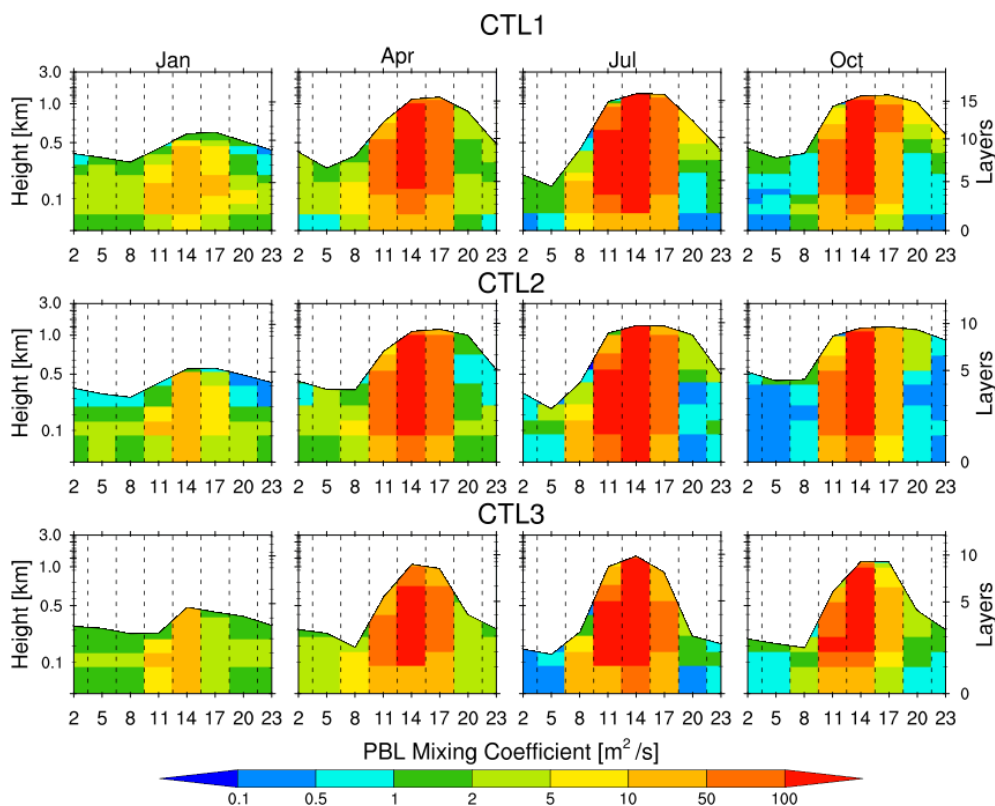
1271
1272 **Figure 6.** Diurnal variation of PBLH and PBL mixing coefficient below PBLH averaged over

1273 Hefei for January, April, July, and October of 2018 from the experiments CTL1, CTL2, and

1274 CTL3.

1275

1276

1277

1278

1279

1280

1281

1282

1283

1284

1285

1286

1287
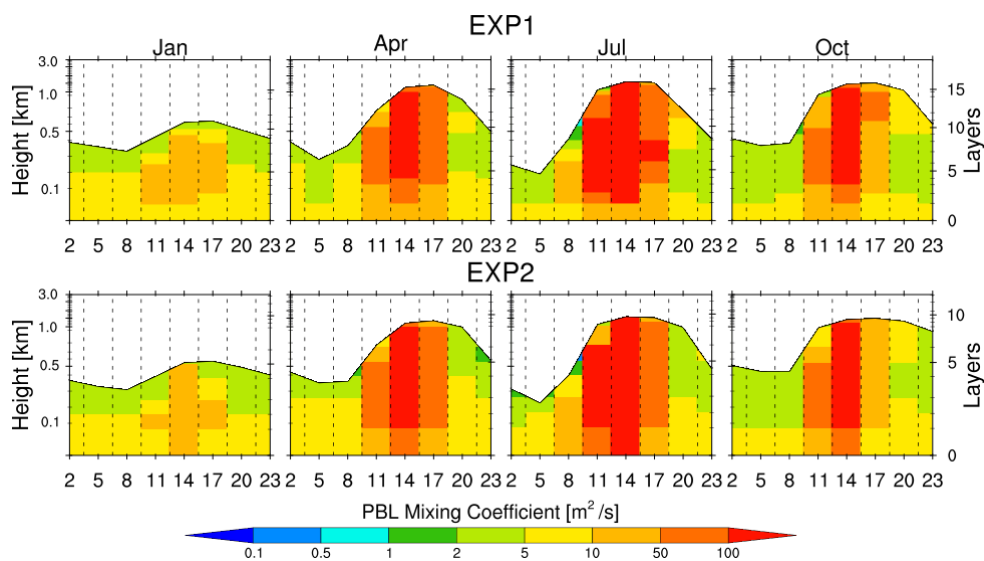
1288

1290 **Figure 7.** Diurnal variation of PBLH and PBL mixing coefficient below PBLH averaged over

1291 Hefei for January, April, July, and October of 2018 from the experiments EXP1 and EXP2.

1292

1293

1294

1295

1296

1297

1298

1299

1300

1301

1302

1303

1304

1305

1306

1307

1308

1309

1310
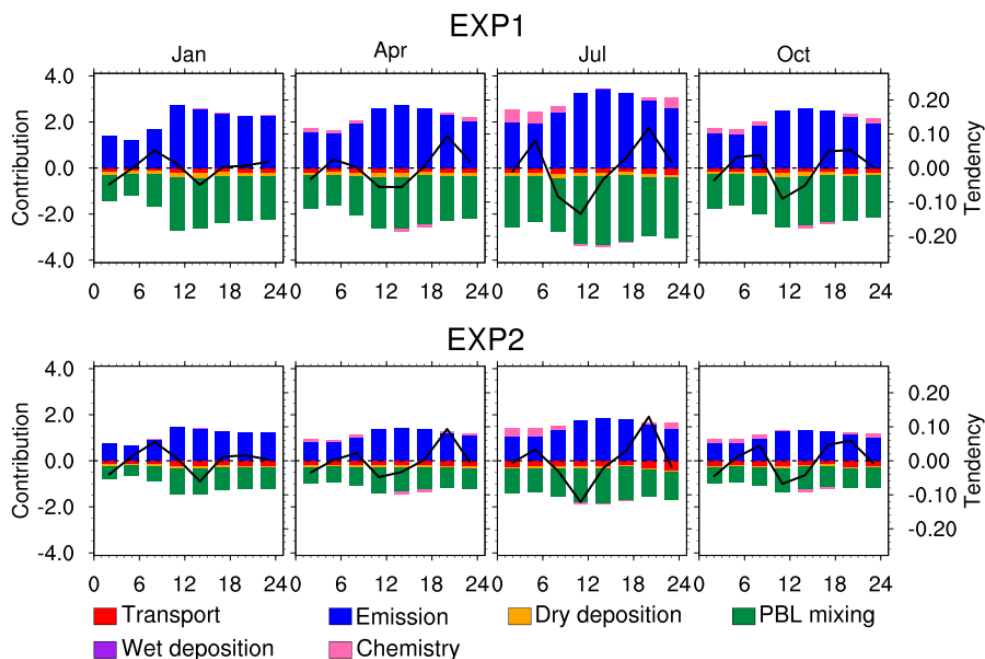
1311

1312 **Figure 8.** Contribution to surface PM$_{2.5}$ concentration every 3-hour from individual processes

1313 (transport, emission, dry and wet deposition, PBL mixing, and chemical production/loss)

1314 averaged over Hefei for January, April, July, and October of 2018 from the experiments EXP1

1315 and EXP2.

1316

1317

1318

1319

1320

1321

1322

1323

1324

1325

1326

1327

1328

1329

1330
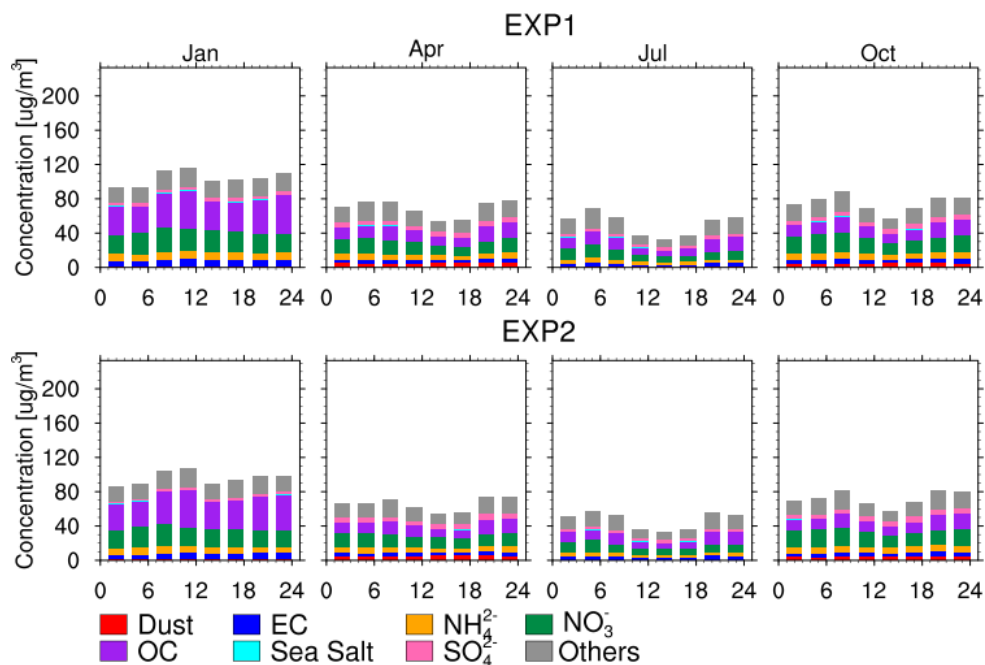
1331
1332 **Figure 9.** Diurnal cycle of surface PM$_{2.5}$ compositions concentration (Dust, OC, EC, Sea Salt,

1333 NH$_4^{2-}$, SO$_4^{2-}$, NO$_3^-$, and other inorganics) averaged over Hefei for January, April, July, and

1334 October of 2018 from the experiments EXP1 and EXP2.

1335

1336

1337

1338

1339

1340

1341

1342

1343

1344

1345

1346

1347

1348

1349

1350
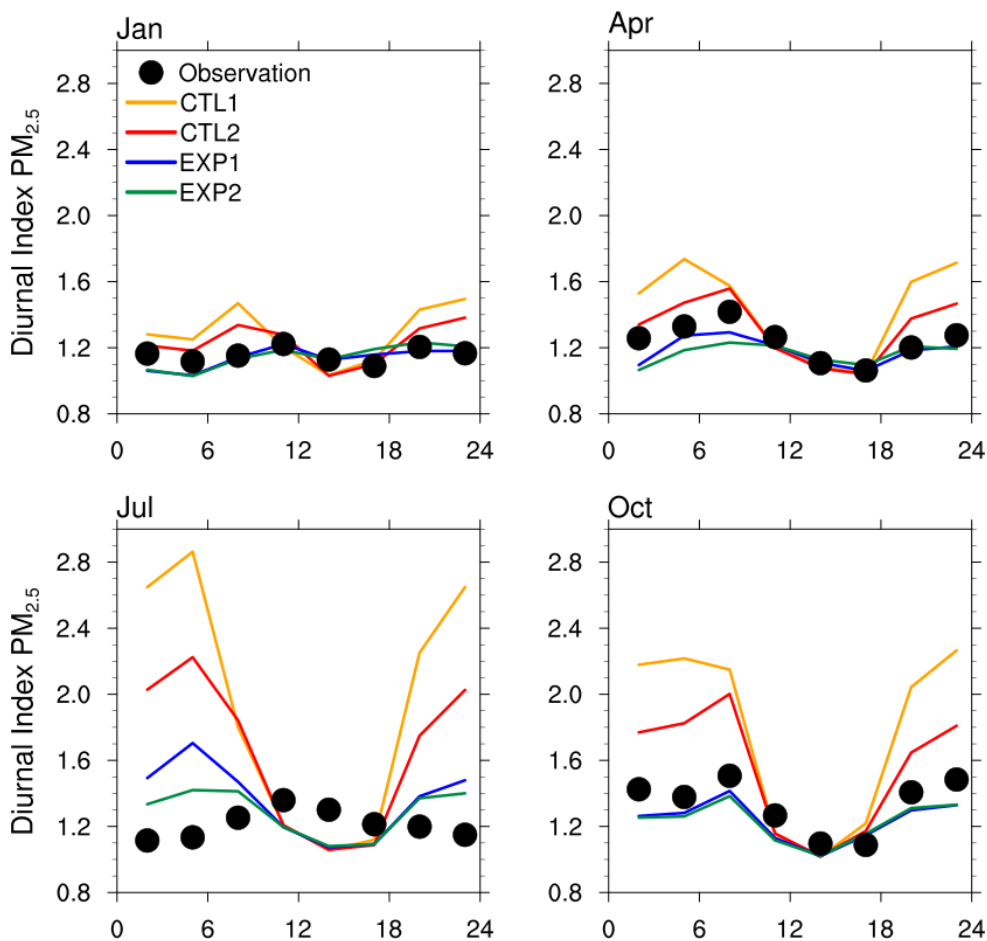
1351
1352 **Figure 10.** Diurnal index of surface PM$_{2.5}$ concentration within 24-hour averaged over the YRD

1353 region of East China (within black box of Fig. 1a) for January, April, July, and October of 2018

1354 from the experiments CTL1, CTL2, EXP1, EXP2, and observations. The simulated results are

1355 from 3-hourly output and sampled at the observational sites.

1356

1357

1358

1359

1360

1361

1362
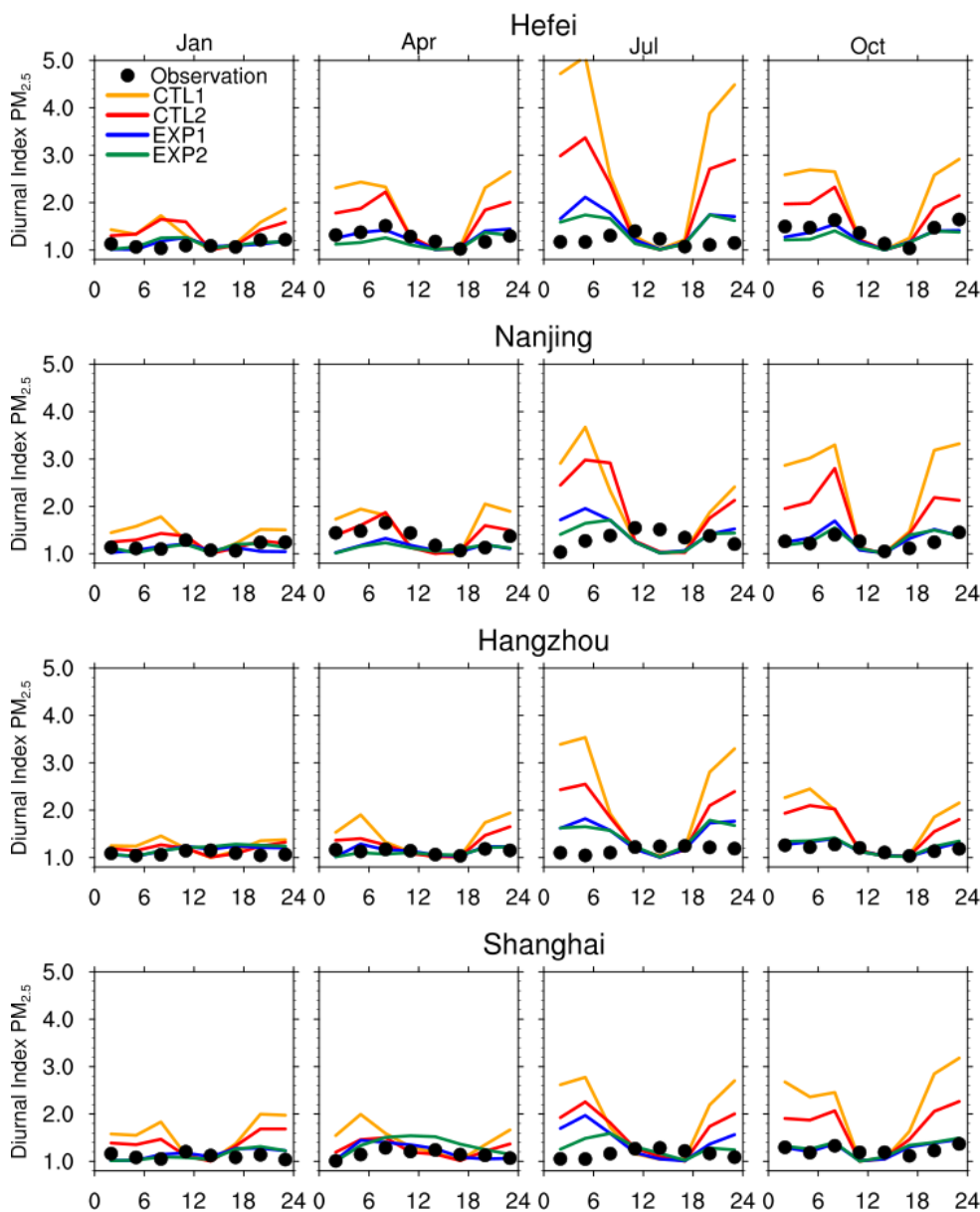
1363

1364 **Figure 11.** Diurnal index of surface PM$_{2.5}$ concentration within 24-hour averaged over four

1365 cities (Hefei, Nanjing, Hangzhou, Shanghai) for January, April, July, and October of 2018 from

1366 the experiments CTL1, CTL2, EXP1, EXP2, and observations.

1367

1368
1369
1370

1371
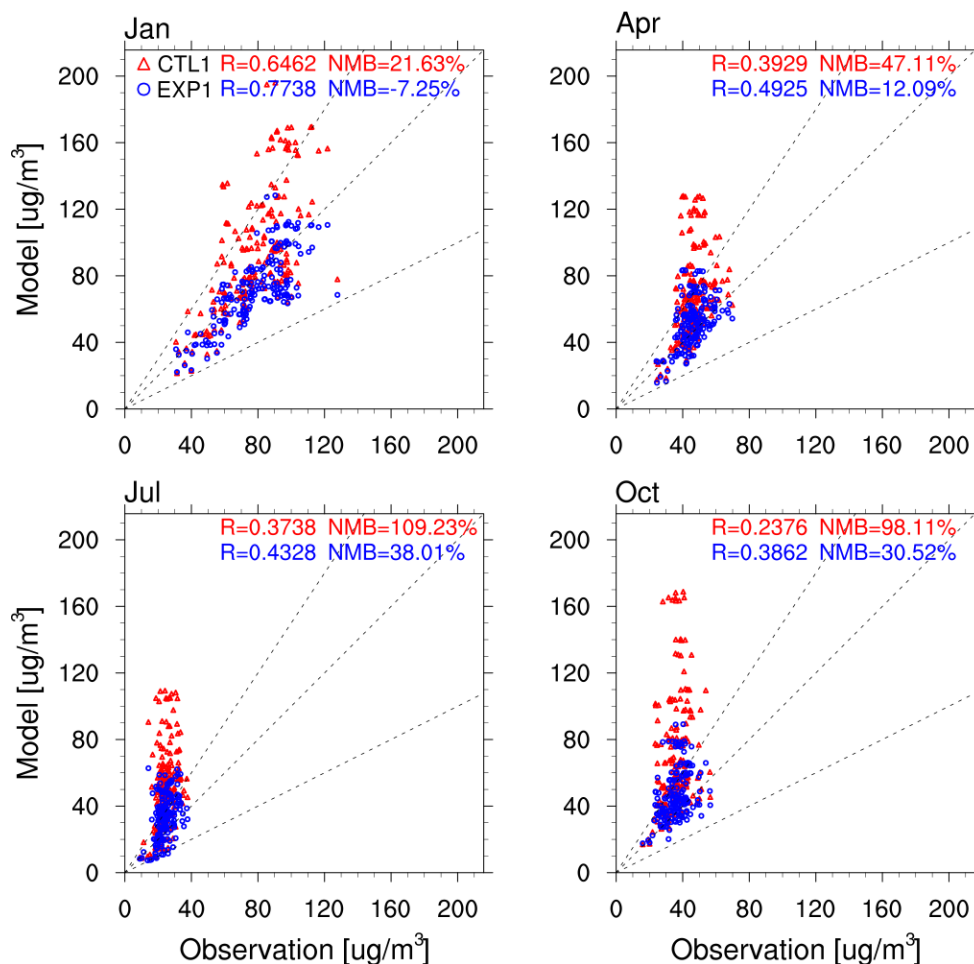
1372
1373 **Figure 12.** Comparison of monthly mean surface PM$_{2.5}$ concentration between the observations

1374 and the simulations from the experiments CTL1 and EXP1 at each observation site over the

1375 YRD region of East China for January, April, July, and October of 2018.

1376

1377

1378

1379

1380

1381

1382

1383
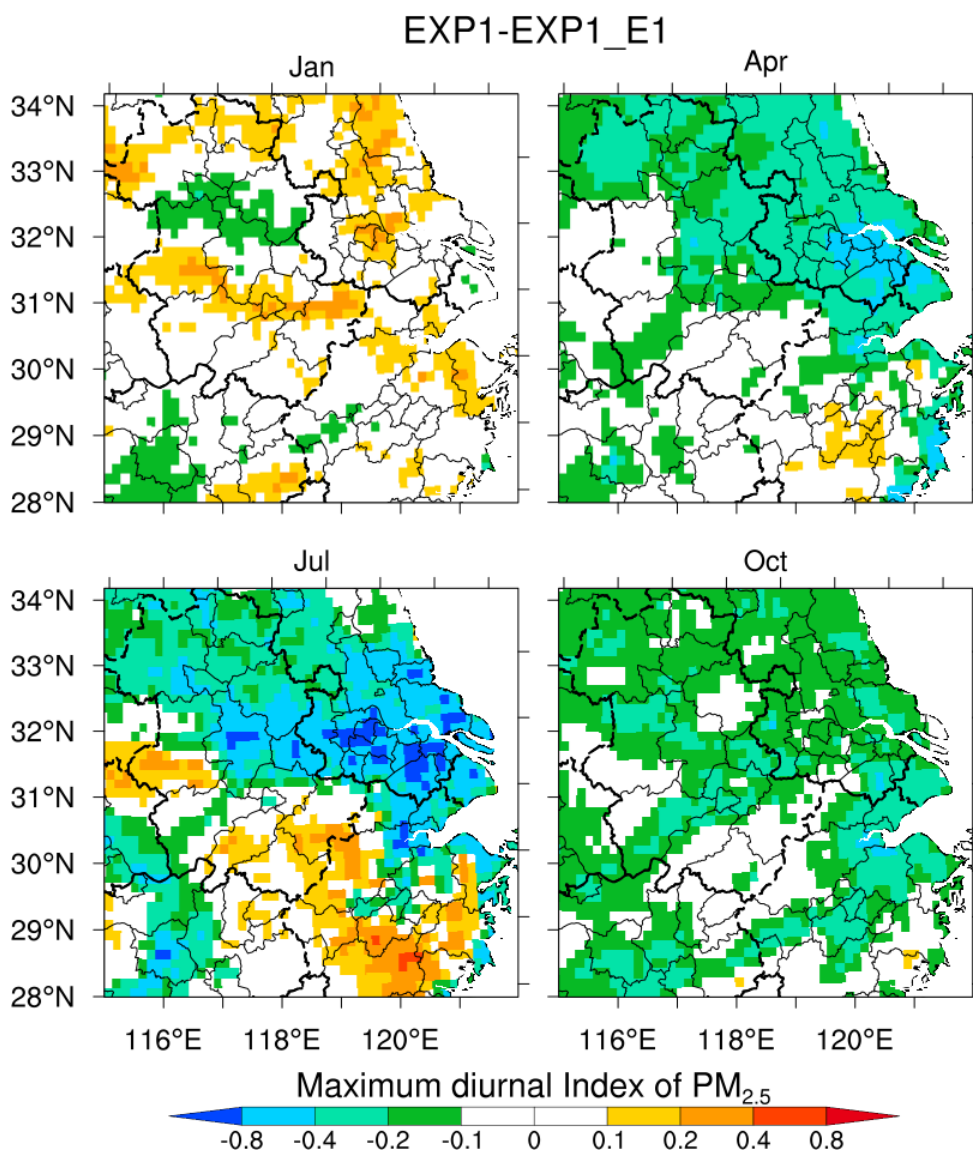
Figure 13. Spatial distribution of the difference in daily maximum diurnal index of surface PM$_{2.5}$ between the experiments EXP1 and EXP1_E1 over East China in January, April, July, and October of 2018.

1391
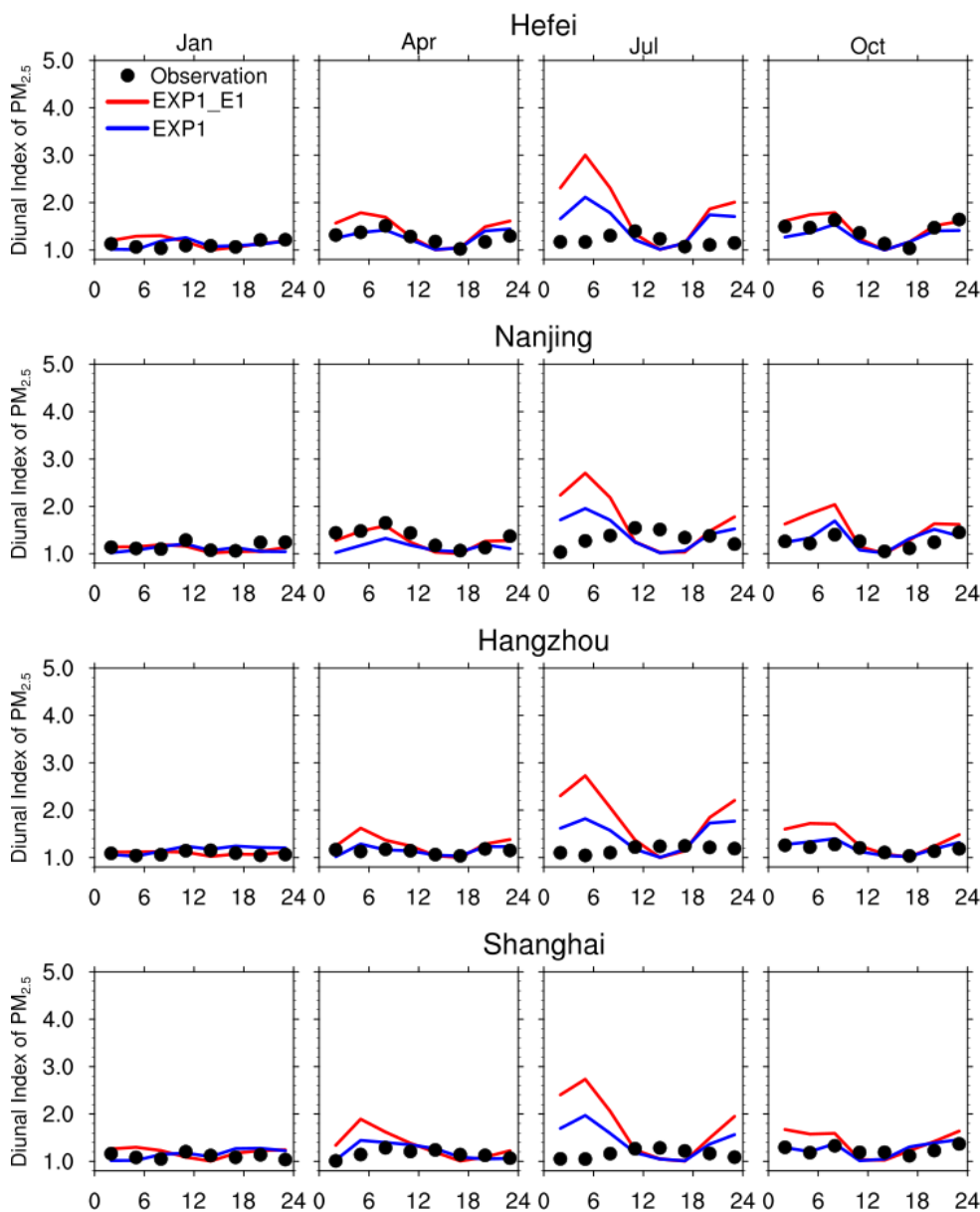
Figure 14. Diurnal index of surface PM$_{2.5}$ concentration within 24-hour averaged over four

cities (Hefei, Nanjing, Hangzhou, Shanghai) for January, April, July, and October of 2018 from

the experiments EXP1_E1, EXP1, and observations.

1399
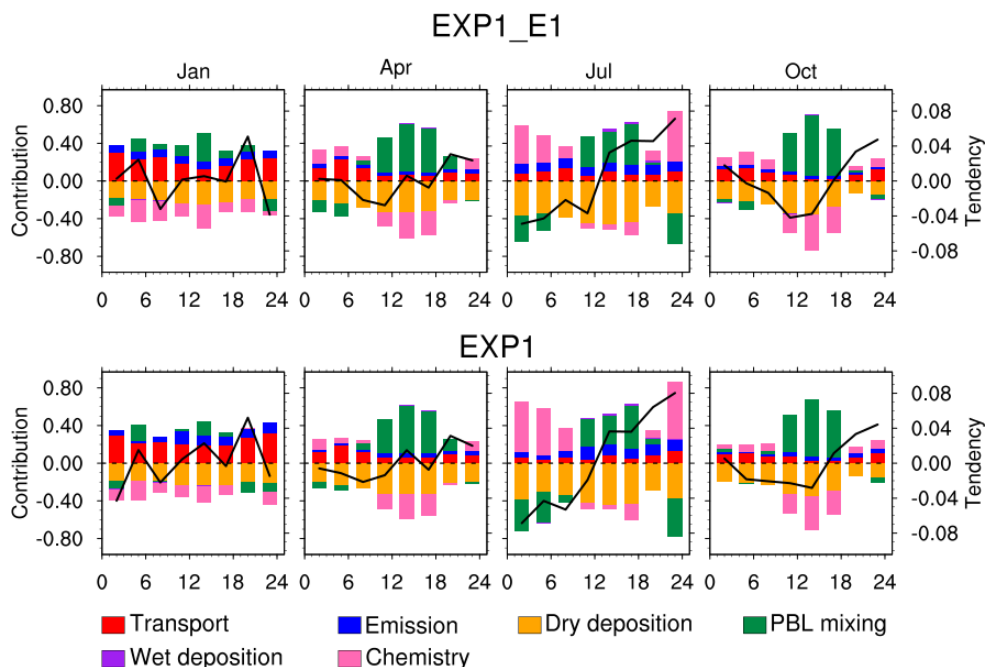
1400
1401 **Figure 15.** Contribution to diurnal variation of surface PM$_{2.5}$ concentration from individual

1402 processes (transport, emission, dry and wet deposition, PBL mixing, and chemical

1403 production/loss) averaged over South Anhui for January, April, July, and October of 2018 from

1404 the experiments EXP1_E1 and EXP1.

1405

1406

1407

1408

1409

1410

1411

1412

1413

1414

1415

1416

1417

1418
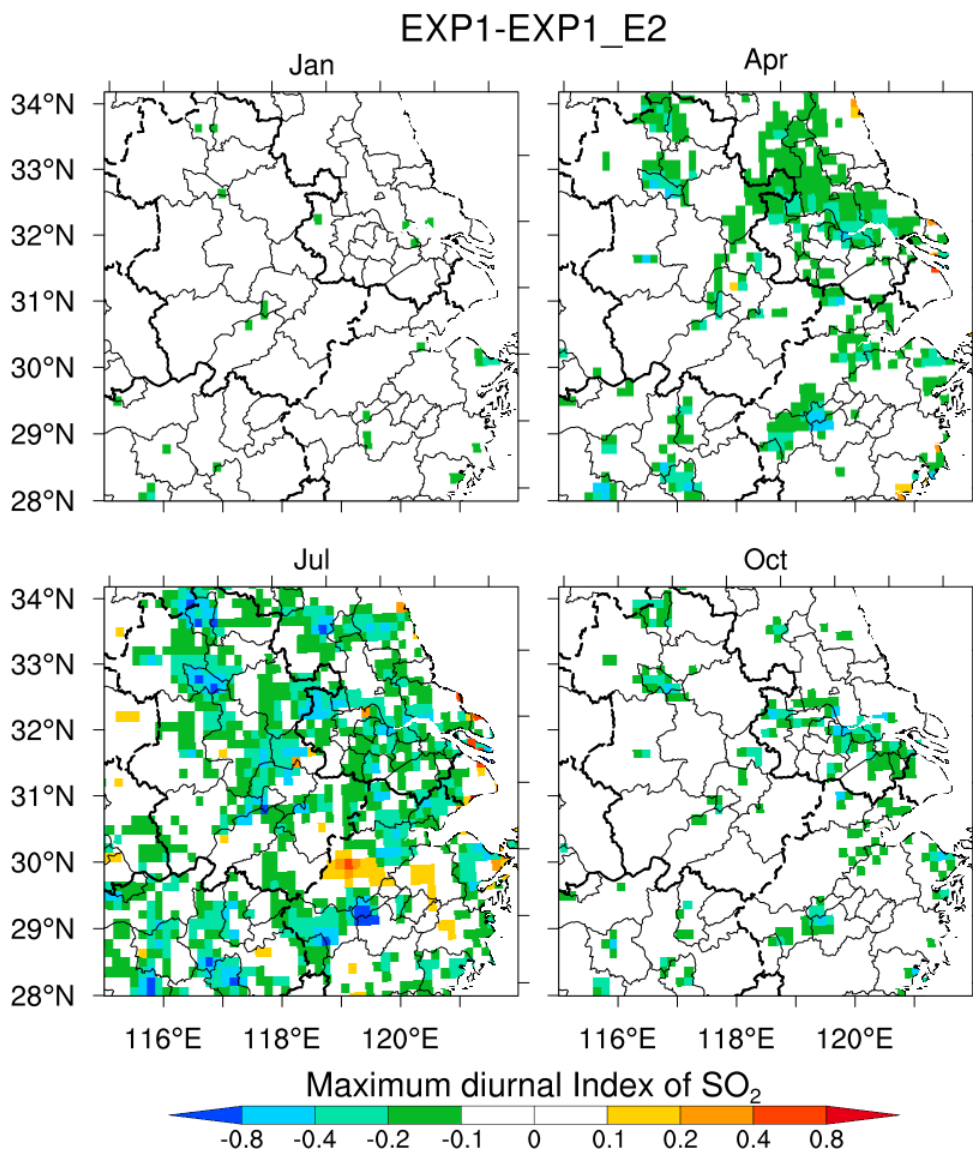
1419
1420 **Figure 16.** Spatial distribution of the difference in daily maximum diurnal index of surface SO_2

1421 between the experiments EXP1_E2 and EXP1 over East China in January, April, July, and

1422 October of 2018.

1423

1424

1425